ISBN 978-82-326-4692-0 (printed version)
ISBN 978-82-326-4693-7 (electronic version)
ISSN 1503-8181

Doctoral Thesis

Jacopo Paglia

Doctoral theses at NTNU, 2020:172

Jacopo Paglia

Statistical modeling for safer drilling operations

NTNU
Norwegian University of
Science and Technology
Faculty of Information Technology
and Electrical Engineering
Department of Mathematical Sciences

NTNU
Norwegian University of
Science and Technology

Doctoral theses at NTNU, 2020:172

NTNU

NTNU
Norwegian University of
Science and Technology

Jacopo Paglia

Statistical modeling for safer drilling operations

Thesis for the degree of Philosophiae Doctor

Trondheim, June 2020

Norwegian University of Science and Technology
Faculty of Information Technology
and Electrical Engineering
Department of Mathematical Sciences

NTNU
Norwegian University of
Science and Technology

NTNU
Norwegian University of Science and Technology

Thesis for the degree of Philosophiae Doctor

Faculty of Information Technology
and Electrical Engineering
Department of Mathematical Sciences

ISBN 978-82-326-4692-0 (printed version)
ISBN 978-82-326-4693-7 (electronic version)
ISSN 1503-8181

Doctoral theses at NTNU, 2020:172

Printed by Skipnes Kommunikasjon as

Preface

The thesis is submitted as partial fulfillment of the requirements of the degree of philosophiae doctor (PhD) at the Norwegian University of Science and Technology (NTNU) in Trondheim. The research, part of the Pressure Ahead Project, has been funded by the Research Council of Norway.

First and foremost, I would like to express my gratitude to my supervisor Jo Eidsvik, for guiding me through the years at NTNU. His invaluable support and advices were of great help for the completion of the thesis. Then I would like to thank my co-supervisor Pierre Cerasi for the inputs he gave me during the meetings we had.
My sincere thanks goes to Ane Lothe, Arnt Grøver, and Juha Karvanen for the help and great contribution on the work carried out together.
I thank the companies and the research institutions involved in the pressure ahead project for the financial support, and for providing most of the data used in my research.
I would also like to thank the Department of Mathematical Sciences at NTNU for the technical, financial, and administrative support.
Finally, I would like to thank Henning Omre for the frequent encouragement and the interesting talks.

Jacopo Paglia
Trondheim, February 11, 2020

Contents

Introduction

The large number of geophysical and geological data available makes the application of statistical methods of primary importance for decision support systems in the earth sciences. The goal of the thesis is to develop models and methodologies to improve data acquisition and assimilation processes in drilling operations. Understanding what type of measurements is needed can help to improve the uncertainty quantification of the variables of interest. The work presented here focuses on application of statistical models in drilling operations, using measurements commonly gathered in the petroleum industry. The following sections introduce the geoscientific and the statistical background of the thesis. The aim is to help the reader to familiarize with terms and notions from petroleum geoscience and statistics. Section 1 introduces the main problems that motivated the thesis. Section 2 contains a description of the concepts and variables involved during the planning of drilling operations. Attention is given to the parameters required for well stability studies. Section 3 describes the statistical methods and techniques used in the study, such as data assimilation, sensitivity analysis and value of information. Finally, Section 4 gives a summary of the papers that compose the thesis, stating their main contribution and discussing possible future works.

1 Motivation

The work is largely inspired by problems related to natural resources characterization such as those in the petroleum industry, with a particular focus on drilling situations. Drilling represents the largest share of the overall operational cost and of the geological risk faced by petroleum companies. Accidents due to a poor study of the well instabilities can have consequences on the economical, environmental and safety level. Drilling a well presents many challenges, mostly due to the uncertainty of the pressure and stress state of the rock formations.

Figure 1 represents an example of a drilling situation. In this case an onshore drilling operation is represented, but the main characteristics

are the same for offshore drilling as well. Here, we present the drill of a well for oil and gas, however the procedures are similar for other drilling purposes, such as water wells or geothermal wells. We have a drilling rig on the surface, that is where the drilling operations are controlled. The subsurface is divided in layers with different types of rock properties (lithology). At shallower depths aquifers are often encountered. It is important at this stage to avoid contamination of the water reservoir, reinforcing the well. As the drilling operations proceed, different types of rock formations can be encountered, depending on the geographical location of the field, and on its geological history. These will greatly affect the drilling speed and the risks faced. Depending for example on whether high pressure formations are encountered, or if we are drilling through faults or extremely hard rocks.

We present a situation where the layers overlying the reservoir are different types of shale. Shale is a soft type of rock with low permeability. At the deepest part the reservoir is found. Hydrocarbons are stored in the porous space of the rocks during geological eras. Rocks with larger permeability, such as sandstone or chalk, are more likely to store hydrocarbon. It is not uncommon anyway to have oil or gas in shale as well. The hydrocarbons are typically sealed in the reservoir by a shale caprock. Figure 1 illustrates a vertical well, straight down into the reservoir. It is also possible to drill wells in other directions, and change direction while drilling. Directional drilling presents even bigger challenges in terms of wellbore stability and larger cost.

2 Drilling a well

Drilling a well is a costly complex operation. It requires appropriate planning to avoid accidents. The risks and cost are much larger in offshore operations, due, for example, to the rough environmental conditions, the difficulty in supplying materials and the limited storage capacity. It is hence important to carefully study the mechanisms that can lead to unwanted issues.

During the drilling of a well there is a redistribution of the stresses in the formation around the borehole wall. This can lead to well instabilities. To balance the stresses, drilling mud is pumped into the wellbore facilitating drilling operations. It helps to keep the borehole open, exerting a pressure on the wellbore wall, and avoiding fluid influx from the formation. Additionally, it cleans the well from cavings, that are rocks of various dimension from the formation originated by borehole wall failure (Fjar et al., 2008). The drilling mud also reduces the possibilities of tools

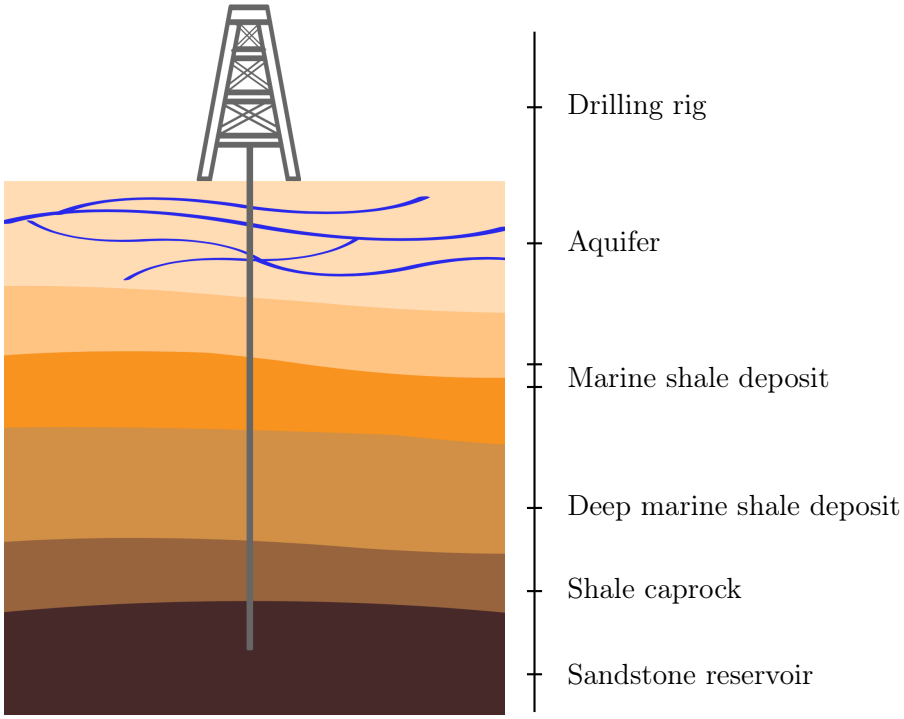

Figure 1: Basic scheme for an oil well. The drilling facilities are located on the surface. At the shallower depths there is an aquifer. Oil is found at the deeper part, most commonly in a sandstone reservoir sealed by a shale caprock (figure adapted from selmandesign.com (2017)).

damages by cooling down the drill bit.

There are hence many factors that need to be taken into consideration when choosing the appropriate mud pressure (p_m). It is possible to control the mud pressure by choosing the adequate mud density (ρ_m) and with the following relation:

$$p_m = \rho_m g Z, \tag{1}$$

where Z is the depth and g is the gravity acceleration constant. The mud pressure has to be high enough to avoid well collapse that can lead to tight hole and stuck pipe, with consequent costly loss of time and problems for other well operations such as logging or cementing. Furthermore, an appropriate choice of mud pressure helps to avoid fluid influx in the well, also called kicks, that in the most dangerous case can lead to blowout, creating large safety and environmental issues. Usually this is controlled

by keeping the mud pressure above the pore pressure (p_p), that is the pressure of the fluids contained in the rocks. Drilling with a pressure lower than pore pressure (underbalanced drilling) can also cause cavings at the borehole wall. At the same time, it is important to keep the mud pressure below the fracture limit, since too large pressure values can re-open natural fractures or initiate new ones with consequent loss of circulation and losses of drilling mud in the formation. That can also lead to kicks and blowout, due to the consequent drop of pressure in the well. The collapse and fracture pressure define respectively the lower and upper limit of the allowable mud pressure. This range of allowed pressures is often called mud weight window (MWW) (Aslannezhad et al., 2016).

Next, we introduce some important criteria used to compute the limit pressures of the MWW. Consider the general case of a vertical well drilled through an impermeable formation in a situation of horizontal stress isotropy. The following is a simplified situation to get familiar with the main criteria used to study well failure, including more details would go beyond the purpose of this introduction.

For the lower limit we study the borehole collapse, that is often due to a shear failure of the formation around the well. We have shear failure when the shear stress exceeds the shear strength of the rock, causing a structural failure with deformations of the borehole wall. The most common method used to study shear failure, and hence collapse of the well, is Mohr-Coulomb (Labuz and Zang, 2012). It can be written using the principal stresses around the well:

$$\sigma_1 = ucs + \sigma_3 \tan^2 \beta, \tag{2}$$

where σ_1 and σ_3 represent respectively the largest and smallest principal effective stresses, obtained by subtracting the pore pressure (multiplied by a factor named Biot coefficient) to the principal stresses. Moreover ucs is the unconfined compressive strength, which is an important parameter that describes the strength of the rock, while β is the failure angle, with $\beta = 45° + \Phi/2$, where Φ is the friction angle, a parameter that describes the ability of rock to resist to the shear stress. From this formulation it is possible to compute the minimum pressure to avoid collapse.

For the upper limit of the MWW it is necessary to compute the fracture pressure. If we are drilling in formations where there are already natural fractures it is enough to exceed the minimum horizontal stress (σ_h) to re-open the fracture (Zoback, 2010). If instead we are drilling an intact formation the pressure necessary to fracture the rock, causing

hence tensile failure is given by

$$p_{frac} = 2\sigma_h - p_p + T_0, \tag{3}$$

where T_0 is the tensile strength which is a parameter that describes the rock strength, and corresponds to the limit for which tensile failure occurs.

Figure 2 shows an example of MWW for a vertical well drilled in the North Sea, for a depth interval that goes from 2470m to 2700 m. The MWW, defined by the lower and upper bound, is plotted together with the pore pressure, the smallest horizontal stress, and the vertical stress (σ_v). The vertical stress also named overburden pressure corresponds to the pressure generated by the weight of the overlying formations. At shallower depths (2470 m and 2530 m) it is safe to drill with a mud pressure lower than the pore pressure, while at larger depths the mud pressure has to be higher than the pore pressure. In this display the upper limit is always larger than the minimum horizontal stress. This may indicate that there are no natural fractures that risk to be re-opened in this depth interval.

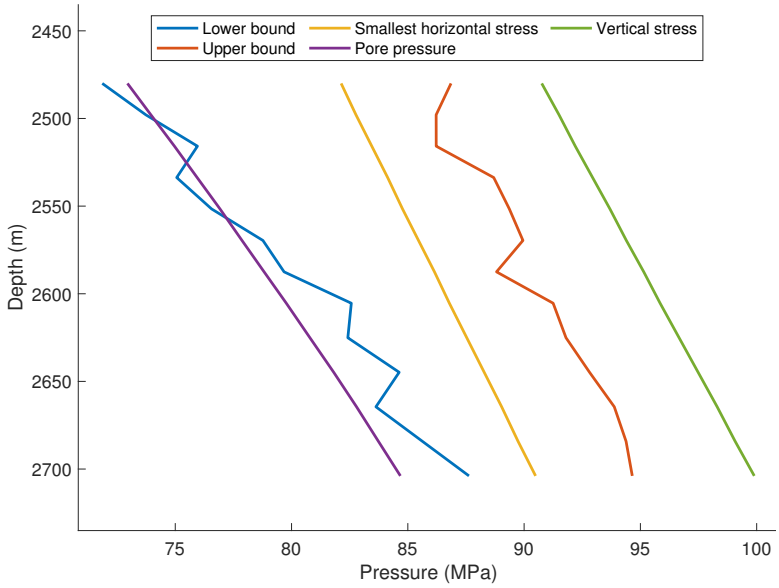

Figure 2: Example of MWW, where the lower and upper limits are plotted together with pore pressure, minimum horizontal stress and vertical stress.

There are some other effects that can impact the computation of the MWW that should also be discussed, in particular we refer to the chemical and thermal effects (Chen et al., 2003). They are included in the study by adding their effect to the tangential and axial principal stresses. The

temperature of the mud can affect the stability of the well: drilling with a mud at a temperature lower than the one of the formation will reduce the risk of well collapse but increase the risk of fracturing. The chemical composition of the mud plays a role as well and there exist two types of drilling fluids: water-based mud and oil-based mud. Oil-based mud gives larger well stability, but for environmental reasons it is often preferred to drill with water-based mud. By reducing the chemical activity of the fluid it is possible to increase the stability of the well. For this reason salt is often added to the drilling fluid. Both thermal and chemical effects are temporary, after some time there will be a situation of equilibrium, with reduced stability.

Well stability software

Well stability in shale can be studied with PSI (Preventing Shale Instabilities). This is a software developed in Sintef. It models the probability of failure of the borehole (Rommetveit et al., 2010; Torsæter and Cerasi, 2015). It also computes the consequent allowed MWW at a given depth or as a function of depth. The MWW is obtained considering the mud densities for which the probabilities of collapse or mud loss are less than a threshold (with a default value of 0.5). Other outputs besides the MWW are: borehole X-section, where the focus is on the stability of the formation around the borehole; stability vs time, where it is possible to monitor the stability of the well as a function of the time since it was drilled.

There exists a large variety of inputs that can be included in PSI. Those can be divided in three main groups:

1. Wellbore data: consisting of information about the well such us well inclination, borehole diameter and mud temperature.

2. Formation conditions: regarding the pressure and stresses of the formation around the borehole. This include pore pressure, vertical and horizontal stresses, and formation temperature (T).

3. Formation properties: regarding the properties of the rock, such as porosity (ϕ), unconfined compressive strength, tensile strength, and friction angle.

Additional information such as lab tests, or the type of mud (oil-based mud or water-based mud) can be included in PSI. It is not necessary to include values for all the parameters to run PSI, the software will compute values for the missing ones from rock physical equations. Figure

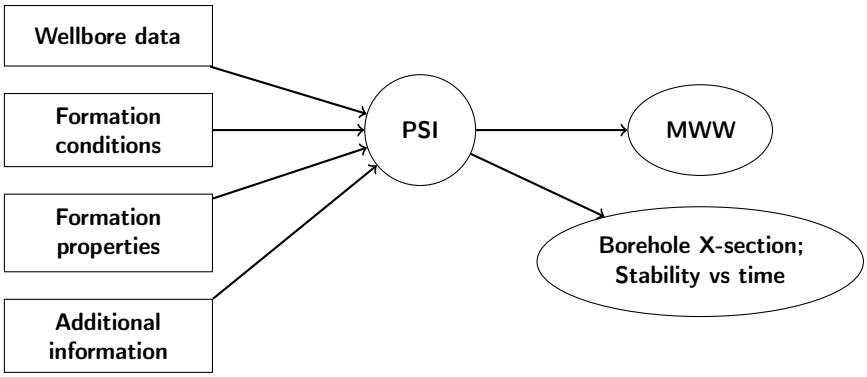

Figure 3: Basic scheme with inputs and outputs for the well stability study in PSI.

3 illustrates a basic scheme for the study of well stability with PSI, with a focus on the input and output parameters. The MWW is computed using the Mohr-Coulomb default criterion (equation (2)). Alternatively it is possible to use other failure criteria: Drucker-Prager, modified Lade, simplified Stassi d'Alia (see e.g. Ulusay (2014); Stassi-D'Alia (1967)).

Pore pressure

Pore pressure is a key parameter to be considered during all the phases of well planning. It is defined as the pressure of the fluid in the porous space of the rock. As mentioned in the previous section pore pressure is central for the computation of the MWW, making particularly relevant the understanding of the mechanisms that lead to pressure instabilities, and the possibility of getting a proper estimation.

The pressure is hydrostatic (or normal pressure) when it corresponds to the weight of a column of water from the surface to a target depth. During geological time compaction and rapid uplift of the formation, can create pressure instabilities, bringing the rock in a state of abnormal pressure. In this situation the fluid will try to flow to reach a state of normal pressure, and this happens quite rapidly in permeable formations such as sandstones. However, in rock formations with low permeability like shales or in permeable formations isolated by faults, the equilibrium state is reached after longer time. In general overpressure is reached when the compaction and uplift are quicker than the time needed for the fluid to flow out of the formation (Rezaee, 2015). Drilling through a formation in abnormal pressure state can be hazardous. In presence of overpressure, for example, there is a higher risks of well collapse and of fluid influx.

Figure 4 shows in black the pore pressure profile in an oil and gas field in the North Sea, the hydrostatic pressure in blue, and the vertical stress in red. The pressure is normal for the first 1500m and then the overpressure starts.

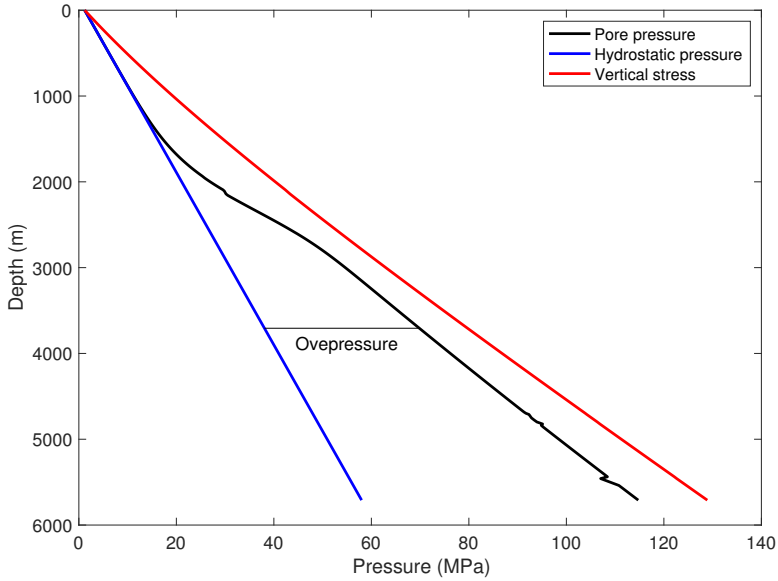

Figure 4: Pore pressure profile together with the hydrostatic pressure and the vertical stress. The pore pressure is normal for the first 1500 m, then it starts to increase entering in an overpressured state.

In the next section we study the most common methods for pore pressure estimation, and in general other types of relevant data measurements for well stability studies.

Data sources

Well logs and lab tests are fundamental in the oil and gas industry (Ellis and Singer, 2007), from exploration to production. Several rock physical relations have been developed over the years to relate the measurements with the quantities of interest (Mavko et al., 2020). We focus only on the measurements that are relevant for drilling operations.

We first look at the possible ways of estimating pore pressure. Direct measurements of pore pressure mainly consist of repeated formation tests (RFT) or drill stem tests (DST). Both these tests measure the pressure of the formation at the borehole wall through a special downhole tool. The RFT is often preferred, being quicker and more accurate. This is

performed by taking a direct sample of the formation fluid. Other types of measurements consist of indirect observations of pore pressure. This is commonly done through data on variables such as resistivity log, sonic log or porosity log. These logs are then related to pore pressure with different equations depending on the type of data, on the location of the field and on the lithology of the formation.

The most common method to get pore pressure values from resistivity is the Eaton equation (Eaton et al., 1975):

$$p_p = \sigma_v - (\sigma_v - p_h)\left(\frac{R}{R_n}\right)^n, \tag{4}$$

where R is the resistivity from the logs, and R_n is the normal resistivity (that is the resistivity at normal pressure). Understanding the electrical resistivity of the formation is important not only for pore pressure estimation, but also to detect the presence of hydrocarbons and to quantify the water saturation. The data are acquired by sending electrical impulses to the formation directly from the borehole wall.

Eaton also introduced a method for estimation of pore pressure from sonic transit time

$$p_p = \sigma_v - (\sigma_v - p_h)\left(\frac{\Delta t_n}{\Delta t}\right)^3, \tag{5}$$

where Δt_n is the sonic transit time at normal pressure, and Δt is the actual transit time log. Sonic transit time is obtained propagating seismic waves into the formation from the borehole, and recording the travel time of the waves. Zhang (2011) extended equations (4) and (5) with a depth dependent normal compaction trend, and derived an equation for pore pressure estimation from porosity logs:

$$p_p = \sigma_v - (\sigma_v - p_h)\frac{\log\phi_0 - \log\phi}{cZ}, \tag{6}$$

where ϕ_0 is the porosity at the seabed. Porosity is estimated from neutron porosity logs, measuring the interactions that neutrons emitted from a source in the borehole, have with the formation. There exist also other possible ways to estimate pore pressure, for example Bowers et al. (1995) introduce a method for pore pressure estimation from sonic velocities.

Before drilling operations start there is however a lack of information about pore pressure. Predrill models are of great help for the drilling engineers (Brahma et al., 2013; El-Werr et al., 2017). The methods are mostly based on interpretation of seismic reflection data.

In addition to the measurements needed to compute pore pressure there are some other well logs that are important to consider when studying well instabilities, such as temperature logs and gamma ray. Gamma rays are used for lithology identification through the quantification of the rock radioactivity. Shale usually has a higher radioactivity than sandstone (Evenick, 2008). Tests performed in the laboratory or directly in the well are particularly relevant. Leak off test and extended leak off test (Addis et al., 1998), are often performed to estimate the minimum horizontal stress and the fracture pressure. The test is performed by initiating a fracture in the formation. It is also possible to obtain samples of the formation rocks when drilling, and performing core analysis.

We focus on the estimation of *ucs*. It is measured by compressing a cylinder of formation sample rock vertically and recording the pressure necessary for cracking it. Although lab tests would be the most reliable way to estimate *ucs*, it can be a quite expensive operation. It is then possible to estimate *ucs* using well measurements (Hassanvand et al., 2018) and drilling data (Hareland et al., 2007). The most common way to estimate *ucs* is using sonic transit time (Oyler et al., 2010). There exists a large number of equations that relate *ucs* with sonic transit time, depending on the type of formation and on the geographical position.

Finally, direct shear test are used to measure the friction angle. The test is applied on samples of formation rocks and it is measured by applying compressive pressure to the samples. Table 1 summarizes the relevant logs and test, describing the type of measurements and which variable is observed.

Geomodeling software

Predrill information about the pressure condition of the formation can be obtained with Pressim (Borge, 2000; Lothe et al., 2004). Pressim is a software developed in Sintef for modeling pressure build-up and release during geological time. Interpreted seismic horizons are used to model the burial history in sedimentary basins. Pressure generation is controlled by burial depth, tectonic activity and chemical and mechanical compaction. The pressure dissipation is controlled by hydraulic leakage and lateral flow. The oil fields taken into consideration are divided into geological compartments separated by faults. Faults and other low permeability barriers control the lateral fluid flow. The model is updated every 1 000 - 10 000 years (Lothe et al., 2019). In this the results at present time are studied. By varying the input parameters it is possible to obtain Monte Carlo realizations of pore pressure. The resulting values of pore pressure are calibrated with direct pressure measurements in the neighboring wells.

Measurement	Variable of Interest	Type
Resistivity log	R	Well log
Neutron porosity log	ϕ	Well log
Sonic log	Δt	Well log
Gamma ray	Lithology	Well log
Temperature log	T	Well log
Repeated formation test	p_p	Formation test
(Extended) leak off test	σ_h	Formation test
Unconfined compression test	ucs	Lab test
Direct shear test	Φ	Lab test

Table 1: Main well logs and tests taken into consideration.

Securing the well

Because of the large risks involved during drilling we focus in this thesis is on the actions necessary to secure the well. The main action taken in this direction is to set casing (Zendehboudi and Bahadori, 2016). This is a procedure used to protect the well from fluid influx and collapse, to avoid formation fracturing, and to prevent sand and other particles from entering the borehole. It is sometimes considered part of the well completion operations. Well completion concerns a range of actions taken during and after drilling a well, to reinforce it and to be able to start production.

The operation is performed by inserting a steel pipe into the wellbore (casing). Cement is then pumped in the space between the casing and the wellbore wall to keep the pipe in place and also provide additional protection to the well. Casing strings consist of steel joints kept together with a casing collar. Usually casing is run in sections during drilling. The well is first drilled at a larger diameter, then the mud is circulated to clean the well, and the drill bit is removed and finally the casing is set. When subsequently a new section of the well is drilled a new string of smaller diameter is inserted in the wellbore. Setting the casing is a costly operation, and deciding the right moment of setting is crucial for maximal drilling speed, since during this casing process the drilling operations are suspended. Moreover, every time a casing is set the diameter of the borehole is reduced, and this could reduce production, with consequent

large economical impact.

The typical scheme of casing is showed in Figure 5. Conductor casing is the first to be set, and it is necessary to support all the further operation, surface casing is often used to protect fresh water zones, intermediate casing is used to protect the well, and finally production casing is set to allow the hydrocarbons to flow into the well via perforations (Adams and Adams, 1985).

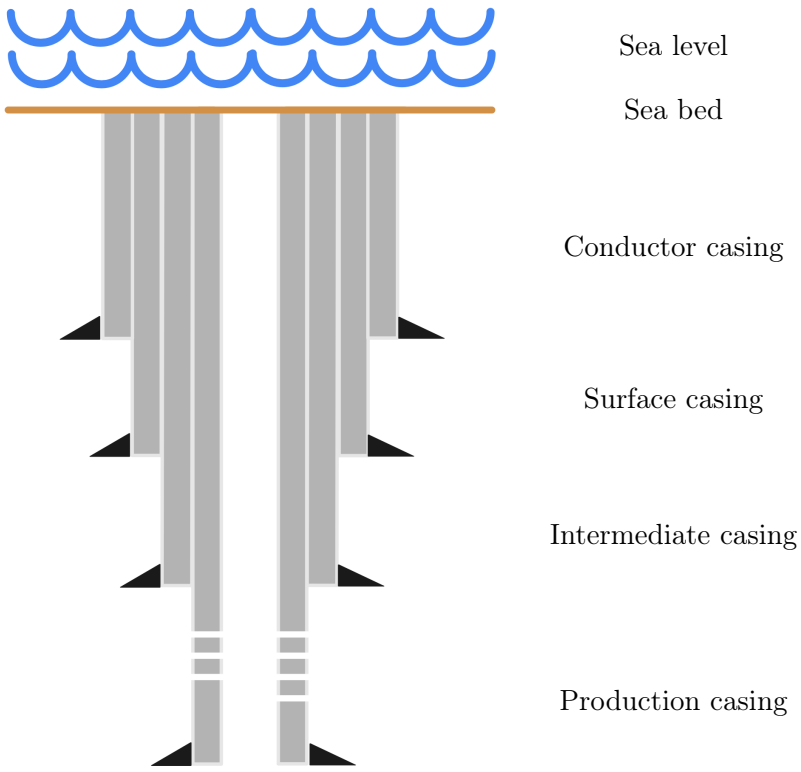

Figure 5: Typical casing scheme, consisting in conductor casing, surface casing, intermediate casing and production casing (figure adapted from selmandesign.com (2017)).

3 Statistical background

Here we discuss the main methodologies used to build statistical models for geoscience, with a particular focus on data assimilation, sensitivity analysis, and decision making. These are important fields of statistics and the aim of the next sections is to provide a background knowledge

of the techniques used in the thesis.

Model building for geoscience

There exists a large variety of methods that can be used when building statistical models for the geosciences. Figure 6 summarizes the main steps we adopt to build our models. The choice of method typically depends

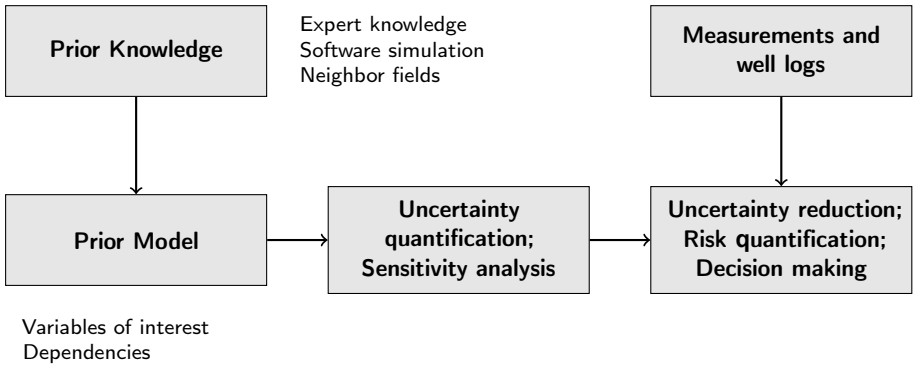

Figure 6: Main steps of the statistical modeling carried out in the thesis.

on the field of application, the type of data available, and the approach chosen by the expert. The amount of data is usually extremely large, they often come from expensive tests and it is crucial to understand how to use them. For doing so we must have in mind the objective of the study, whether it concerns to model well stability, reservoir management or oil exploration surveying, for example. Because the work presented in this thesis is mostly based on drilling situations, we will only discuss the data and techniques used in this field of application. Some of the available information is used to model the variables of interest, understand the uncertainties, and model the dependencies. In most of the cases that kind of information comes from prior knowledge obtained from a combination of expert knowledge, information from similar oil fields and software simulations.

Without going into technical details, we will next define a minimum of notation to describe some key concepts. Consider a situation with a phenomenon x distributed over a spatial domain, and $\boldsymbol{s}$ being the coordinates in a multidimensional space. As initial step it is important to understand the global trend of the variable we are interested in, modeling the expected value $\mathbb{E}\left[x(\boldsymbol{s})\right]$ at different locations $\boldsymbol{s}$ of the spatial domain. This is often done by fitting a regression model, that does not need to be

linear, including knowledge about important covariates, such as depth, geological compartment, and type of layer. Next, when building a statistical model often one needs some way to capture correlations in space, which later allows the propagation of information from one location to the others. Variograms are often used in this context in geostatistics (Oliver and Webster, 2014). Understanding and fitting the appropriate variogram will be helpful to construct the covariance matrix. The variogram is defined as the variance of the difference of the values of the random field at distance $\boldsymbol{h}$ (Matheron, 1963), $\gamma(\boldsymbol{h}) = \frac{1}{2}\text{Var}\left[x(\boldsymbol{s}) - x(\boldsymbol{s}+\boldsymbol{h})\right]$. The empirical variogram is used to estimate the variogram from the available data, and it is computed with

$$\hat{\gamma}(\boldsymbol{h}) = \frac{1}{2N_{loc}(\boldsymbol{h})} \sum_{i \in N_{loc}(h)} \left(x(\boldsymbol{s}_i) - x(\boldsymbol{s}_i + \boldsymbol{h})\right)^2 \tag{7}$$

where $N_{loc}(\boldsymbol{h})$ the number of locations at distance $\boldsymbol{h}$ from each other. We use the variogram information to fit probability distributions or stochastic processes, often assuming a Gaussian process for the variables of interest. In this way, one can fit a Gaussian process to a surrogate complex physical model (Gramacy, 2020; Su et al., 2017).

Sensitivity analysis and uncertainty quantification can be useful at this stage, since they help to get a better understanding of how the uncertainties propagate, and finding out what are the variables with larger effects on the results.

The initial statistical model should be updated when more of the petroleum measurements are available. This can be done by data assimilation with the final objective of improved prediction and uncertainty quantification, and for decision making. Data are then sequentially assimilated in the model for a better knowledge of the variable, they help for risk quantification, and to improve the data gathering scheme. In the next sections we discuss the topic of data assimilation, sensitivity analysis, and decision making in more details.

Data assimilation

We now discuss about the problem of assimilating observations for uncertainty quantification of a spatially distributed phenomenon. We introduce data assimilation in a general framework for a more complete discussion. Consider the problem of state estimation for a spatially distributed phenomenon that evolves in time $\boldsymbol{x} = (\boldsymbol{x}_0, ..., \boldsymbol{x}_T)$, for example here $\boldsymbol{x}_t$, $t = 0, \ldots, T$ denotes a vector of variable allocated to spatial locations at fixed time t. We are not able to directly observe the phenomenon, but we

can obtain noisy measurements $\boldsymbol{d} = (\boldsymbol{d}_0, ..., \boldsymbol{d}_T)$ at each time. We aim to derive the state of the system from the measurements. It is possible to estimate the distribution of the latent variable $\boldsymbol{x}$ given the measurements using the classical Bayes' rule:

$$p(\boldsymbol{x}|\boldsymbol{d}) = \frac{p(\boldsymbol{x})p(\boldsymbol{d}|\boldsymbol{x})}{p(\boldsymbol{d})}. \tag{8}$$

Where $p(\boldsymbol{x})$ is the prior distribution of $\boldsymbol{x}$, $p(\boldsymbol{d}|\boldsymbol{x})$ is the likelihood model, and $p(\boldsymbol{d})$ is the normalizing constant computed from $\int p(\boldsymbol{d}|\boldsymbol{x})p(\boldsymbol{x})\mathrm{d}\boldsymbol{x}$, considering a continuous sample space for $\boldsymbol{x}$. Assume that the phenomenon described by the latent variable $\boldsymbol{x}$, is a first order Markov process, so that the distribution of the state $\boldsymbol{x}_t$ only depends on the distribution of $\boldsymbol{x}_{t-1}$

$$p(\boldsymbol{x}_t|\boldsymbol{x}_{t-1}, ..., \boldsymbol{x}_0) = p(\boldsymbol{x}_t|\boldsymbol{x}_{t-1}), \tag{9}$$

and the joint distribution can be written as

$$p(\boldsymbol{x}) = p(\boldsymbol{x}_0)p(\boldsymbol{x}_1|\boldsymbol{x}_0) \cdots p(\boldsymbol{x}_t|\boldsymbol{x}_{t-1}) \tag{10}$$

Furthermore, at each time t, consider that we can obtain the measurement $\boldsymbol{d}_t$ that, assuming conditional independence, allows us to write the likelihood distribution as

$$p(\boldsymbol{d}|\boldsymbol{x}) = \prod_{t=0}^{T} p(\boldsymbol{d}_t|\boldsymbol{x}_t). \tag{11}$$

This will define an hidden Markov model (Figure 7).

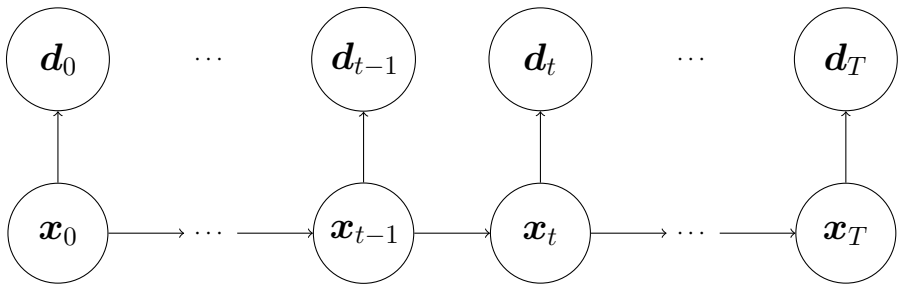

Figure 7: Hidden Markov model where $\boldsymbol{x}$ is the latent variable and $\boldsymbol{d}$ the measurements.

Data assimilation techniques allow the inclusion of data in the model to obtain a better knowledge of the state of the system. The classical example of data assimilation methodology is from meteorology where

the problem of making better forecast based on large amounts of data is particularly relevant. Data assimilation is now used in several areas of geoscience, such as petroleum resources characterization (Fletcher, 2017). Combining model forecast and observations, it can be seen as an inverse problem (Lahoz and Menard, 2010). In our case the inversion problem takes the shape of Bayesian inversion. It is possible to divide the inverse problem, in filtering, smoothing, and prediction. In filtering the interest is in getting the current state ($\boldsymbol{x}_t$) given all the measurements up to time t ($\boldsymbol{d}_0, ..., \boldsymbol{d}_t$), that in terms of probability distributions means $p(\boldsymbol{x}_t|\boldsymbol{d}_t, ..., \boldsymbol{d}_0)$. Smoothing consists in estimating of states ($\boldsymbol{x}_t, ..., \boldsymbol{x}_s$) with $0 \leq s \leq t \leq T$, using all the measurements available, hence computing $p(\boldsymbol{x}_t, ..., \boldsymbol{x}_s|\boldsymbol{d}_T, ..., \boldsymbol{d}_0)$. Finally with prediction the attention is on getting an estimate of the future states of the system given the measurements up to present time, hence $p(\boldsymbol{x}_{t+k}|\boldsymbol{d}_t, ..., \boldsymbol{d}_0)$, with $k = 1, ..., T - t$ (Särkkä, 2013; Asch et al., 2016).

For our goal of real time estimation of a spatially distributed phenomenon we use filtering algorithms, focusing then only on the measurements collected up to the current time. The Kalman filter is one of the most known filtering algorithm (Kalman, 1960). Working with hidden Markov models helps to derive the Kalman filter steps. Under the additional assumptions of a linear Gaussian model, the Kalman filter enables the explicit computation of the posterior distribution of the state, that will be Gaussian, by estimating the mean and the variance (Myrseth and Omre, 2010). We first define the linear Gaussian forward model and likelihood using the properties of the hidden Markov model

$$\begin{aligned} \left[\boldsymbol{x}_t|\boldsymbol{x}_{t-1}\right] &= \boldsymbol{A}_{t-1}\boldsymbol{x}_{t-1} + \boldsymbol{\epsilon}^x_{t-1}, & \boldsymbol{\epsilon}^x_{t-1} &\sim N\left(0, \boldsymbol{Q}_{t-1}\right), \\ \left[\boldsymbol{d}_t|\boldsymbol{x}_t\right] &= \boldsymbol{H}_t\boldsymbol{x}_t + \boldsymbol{\epsilon}^d_t, & \boldsymbol{\epsilon}^d_t &\sim N\left(0, \boldsymbol{R}_t\right), \end{aligned}$$

and the initial distribution at $t = 0$, $\boldsymbol{x}_0 \sim N\left(\boldsymbol{\mu}_0, \Sigma_0\right)$. Here $N(\boldsymbol{\mu}, \boldsymbol{\Sigma})$ denotes a normal random variable with mean vector $\boldsymbol{\mu}$, and covariance matrix $\boldsymbol{\Sigma}$. We can recursively compute the mean and covariance of the states $\boldsymbol{x}_t$, $t = 1, ..., T$ through a prediction and an update step.

Prediction:

$$\boldsymbol{\mu}^p_t = \boldsymbol{A}_{t-1}\boldsymbol{\mu}_{t-1}, \tag{12}$$

$$\boldsymbol{\Sigma}^p_t = \boldsymbol{A}_{t-1}\boldsymbol{\Sigma}_{t-1}\boldsymbol{A}'_{t-1} + \boldsymbol{Q}_{t-1}. \tag{13}$$

Update:

$$\boldsymbol{\mu}_t = \boldsymbol{\mu}^p_t + \boldsymbol{\Sigma}^p_t\boldsymbol{H}'_t\left(\boldsymbol{H}_t\boldsymbol{\Sigma}^p_t\boldsymbol{H}'_t + \boldsymbol{R}_t\right)^{-1}\left(\boldsymbol{d}_t - \boldsymbol{H}_t\boldsymbol{\mu}^p_t\right), \tag{14}$$

$$\boldsymbol{\Sigma}_t = \boldsymbol{\Sigma}^p_t - \boldsymbol{\Sigma}^p_t\boldsymbol{H}'_t\left(\boldsymbol{H}_t\boldsymbol{\Sigma}^p_t\boldsymbol{H}'_t + \boldsymbol{R}_t\right)^{-1}\boldsymbol{H}_t\boldsymbol{\Sigma}^p_t. \tag{15}$$

In a static case, hence without forward model, accurate measurements give a reduction of the estimated variance at the location where data are collected.

The method has been extended taking into account non linearity of the likelihood and to deal with ensembles rather than a parametric prior distribution (Evensen, 2009). The extended Kalman filter covers the case of minor non-linearity, approximating the likelihood and forward model with a first order Taylor expansion. Consider a non linear forward model and a non linear likelihood

$$\left[\boldsymbol{x}_t|\boldsymbol{x}_{t-1}\right] = \mathbf{f}_{t-1}\left(\boldsymbol{x}_{t-1}\right) + \boldsymbol{\epsilon}^x_{t-1}, \qquad \boldsymbol{\epsilon}^x_{t-1} \sim N\left(0, \boldsymbol{Q}_{t-1}\right), \tag{16}$$

$$\left[\boldsymbol{d}_t|\boldsymbol{x}_t\right] = \boldsymbol{h}_t\left(\boldsymbol{x}_t\right) + \boldsymbol{\epsilon}^d_t, \qquad \boldsymbol{\epsilon}^d_t \sim N\left(0, \boldsymbol{R}_t\right). \tag{17}$$

Again it is possible to estimate the state distribution by approximating the mean and the covariance.

Prediction:

$$\boldsymbol{\mu}^p_t = \mathbf{f}_{t-1}\left(\boldsymbol{\mu}_{t-1}\right), \tag{18}$$

$$\boldsymbol{\Sigma}^p_t = \boldsymbol{F}_{t-1}\left(\boldsymbol{\mu}_{t-1}\right)\boldsymbol{\Sigma}_{t-1}\boldsymbol{F}_{t-1}\left(\boldsymbol{\mu}_{t-1}\right)' + \boldsymbol{Q}_{t-1}. \tag{19}$$

Update:

$$\boldsymbol{\mu}_t = \boldsymbol{\mu}^p_t + \boldsymbol{\Sigma}^p_t\boldsymbol{H}'_t\left(\boldsymbol{\mu}^p_t\right)\left(\boldsymbol{H}_t\left(\boldsymbol{\mu}^p_t\right)\boldsymbol{\Sigma}^p_t\boldsymbol{H}'_t\left(\boldsymbol{\mu}^p_t\right) + \boldsymbol{R}_t\right)^{-1}\left(\boldsymbol{d}_t - \boldsymbol{h}_t\left(\boldsymbol{\mu}^p_t\right)\right), \tag{20}$$

$$\boldsymbol{\Sigma}_t = \boldsymbol{\Sigma}^p_t - \boldsymbol{\Sigma}^p_t\boldsymbol{H}'_t\left(\boldsymbol{\mu}^p_t\right)\left(\boldsymbol{H}_t\left(\boldsymbol{\mu}^p_t\right)\boldsymbol{\Sigma}^p_t\boldsymbol{H}'_t\left(\boldsymbol{\mu}^p_t\right) + \boldsymbol{R}_t\right)^{-1}\boldsymbol{H}_t\left(\boldsymbol{\mu}^p_t\right)\boldsymbol{\Sigma}^p_t. \tag{21}$$

Here $\boldsymbol{F}_{t-1}$ and $\boldsymbol{H}_t$ are the Jacobian of the functions $\mathbf{f}_{t-1}$ and $\boldsymbol{h}_t$ respectively. There are some limitations in using the extended Kalman filer. The main problem comes from the non existence of the Jacobian matrix, and this can happen in the presence of not differentiable functions. Additionally, assuming that it is possible to compute the Jacobian matrix, it can happen that a linear approximation of the functions differ too much from the functions itself affecting the state estimation (Julier and Uhlmann, 2004).

Sensitivity analysis

Sensitivity analysis is an important tool to study the effect of the input parameters on a given model. Sensitivity analysis can also be used to study how the uncertainty in the model outputs is related to the

uncertainty in the inputs. It allows the classification of the inputs based on their main effects and their interaction effects. There are numerous approaches for sensitivity analysis. Iooss and Lemaître (2015) give an overview on the most used methods for global sensitivity analysis.

The one-at-the-time methods are a family of techniques where every time only one parameter varies while the others are kept fixed. The most important technique is the Morris method (Morris, 1991). The algorithm, works well for large dimensions and allows the computation of the main effects, letting the parameters vary in a discrete space. Campolongo et al. (2007) propose an improved version of the Morris method, where a new and more efficient version of Morris' measure is introduced, enabling one to work with groups of variables. Particularly useful as a screening technique is the method proposed by Sacks et al. (1989) where a stochastic approach is used to model inputs and outputs, making it easier to work with uncertainties in the inputs. Fruth et al. (2015) introduce a sequential method for sensitivity analysis to study the effects of scalar and functional inputs on an expensive experiment. The method sequentially divides the domain of the functional in smaller subdomains, focusing on the most interesting ones. Regression analysis is used do define the sensitivity indexes.

In a different flavor the variance based methods (Saltelli et al., 2008), decompose the variance of the output in functions that depends on the single inputs and on combinations of them. Working with variances makes it more intuitive to study how uncertainties in the inputs are propagated in the outputs.

To exemplify one sensitivity method, we briefly describe the Sobol indexes (Sobol, 1993, 2001) which are extremely useful to understand how the variance of the output (y) is affected by the variance of inputs ($\boldsymbol{x} = (x_1, ..., x_k)$). We consider then y to be function of $\boldsymbol{x}$ ($y = f(x_1, ..., x_k)$). The Sobol indexes give the possibility to study main effect of every inputs and the higher order effects. They are estimated using a method proposed in Saltelli et al. (2010). We first need to generate two independent sample matrices $\boldsymbol{A}$ and $\boldsymbol{B}$ ($n \times k$) of input values from the defined distribution of $\boldsymbol{x}$, where k is the number of inputs, and n is the number of samples. That means that each row of $\boldsymbol{A}$ and $\boldsymbol{B}$ is a realization of $(x_1, ..., x_k)$. In addition consider the matrices $\boldsymbol{M}_i$, $i = 1, ..., k$, obtained from $\boldsymbol{B}$, replacing the i_{th} column with the i_{th} column of $\boldsymbol{A}$. The main effects SB_i

are estimated with

$$SB_i = \frac{\mathrm{Var}\left(\mathbb{E}\left(y|x_i\right)\right)}{\mathrm{Var}\left(y\right)} \approx \frac{\mathrm{Var}\left(y\right) - \frac{1}{2n}\sum_{j=1}^{n}\left(f(\boldsymbol{A})_j - f(\boldsymbol{M}_i)_j\right)^2}{\mathrm{Var}\left(y\right)} = 1 - \frac{\frac{1}{2n}\sum_{j=1}^{n}\left(f(\boldsymbol{A})_j - f(\boldsymbol{M}_i)_j\right)^2}{\frac{1}{n}\sum_{j=1}^{n}\left(f(\boldsymbol{A})_j\right)^2 - \left(\frac{1}{n}\sum_{j=1}^{n} f(\boldsymbol{A})_j\right)^2}, \quad i = 1, ..., k. \tag{22}$$

Where $f(\boldsymbol{A})_j$ (and $f(\boldsymbol{B})_j$) means that the function f has been evaluated at the j_{th} row of $\boldsymbol{A}$ (or $\boldsymbol{B}$). The main effect expresses then what proportion of the variance of the output is due to the variance of the input. As an extension of the Sobol method, Iooss and Prieur (2017) suggest to use the Shapley effect for sensitivity analysis when there is statistical dependency between the inputs. Mara and Tarantola (2012) also study the case of dependent inputs presenting indexes for non linear dependency.

Finally, Fenwick et al. (2014) propose a method for sensitivity analysis that can find important applications in geoscience. The method, called distance based sensitivity analysis (Park et al., 2016), divides the model responses into classes and finds out what parameters are responsible for the division. The number of classes is chosen using the silhouette index (Rousseeuw, 1987), that assigns a value describing how well each model response fits into the classes. It is computed with

$$SI(i) = \frac{b(i) - a(i)}{\max\{a(i), b(i)\}}, \tag{23}$$

where $a(i)$ is the average distance between the response and all the other objects in the class, and $b(i)$ the minimum average distance between the response and all the objects in the other classes. $SI(i)$ takes values between in $[-1, 1]$ and larger values indicates better fits in the class. To divide the responses in classes a k-medoids clustering algorithm is typically used. The algorithm finds the clustering configurations that minimizes the distances between the objects in each class and the object selected as a center. Once the responses are assigned to the classes the empirical cumulative distribution function of each parameter is computed in each class and over the entire sample, the L^1 distance between the empirical cumulative distributions will then be the measure of the main effect of the parameters. Similarly it is possible to compute the interactions, looking at the conditional cumulative distribution between the parameters in each class and over the all sample.

Figure 8 illustrates an application of the distance based sensitivity analysis. The figure shows the computed empirical cumulative distributions in each class and for all samples. Figure 8a shows a parameter with

a large main effect compared to the one in Figure 8b. This is evident looking at the distances between the cumulative distribution functions, which almost fall on top of each other in Figure 8b, showing that parameter 2 has negligible effect on the output response.

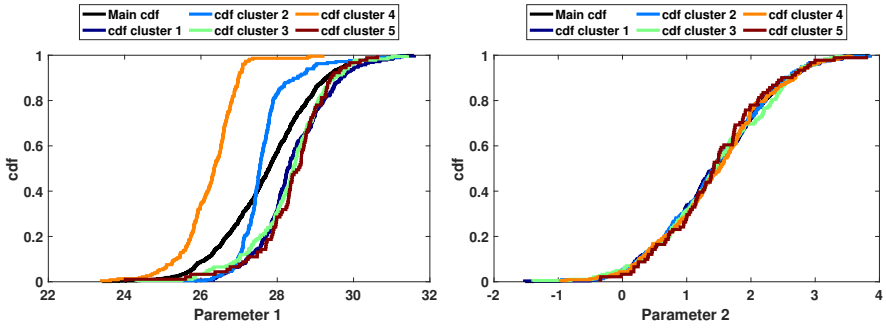

(a) Parameter with large main effect. (b) Parameter with low main effect

Figure 8: Example of computation of main effects using the distance based global sensitivity analysis.

Decision making

Making decisions is not an easy task, here many factors have to be taken into consideration. The decision maker has to study the possible outcomes of each decision and then go for the one that will give the best value. Several difficulties are faced here, Bratvold and Begg (2010) identify uncertainty of the information, together with complexity of the problem as some of the main sources of difficulties that a decision maker has to face.

Decision trees are often used to model and visually describe the decision situation. They consist of tree diagrams where square nodes represent the decision node, circle nodes represent the uncertainties, and the leaves are the value results. Each of the outcome of an uncertainty node is associated with a probability. The decision maker can then choose the best alternative by solving the tree. We consider a situation with a risk neutral decision maker, meaning that the scope is to choose the alternative that maximizes the expected profit. We illustrate a situation with a small size tree which is solved by starting from the leaves and computing the expected value, and then choosing the alternative that gives the largest expected value. Figure 9 shows this example of a decision related to a drilling situation. Here, the decision maker is free to choose between three possible alternatives: keep drilling, run casing, and quit. Solving

the tree we can see that the best alternative is to keep drilling, since in this situation it gives the largest expected value ($\$ - 360\ 000$). In this illustration, it is naturally a rather simple decision situation, and in more difficult cases it will involve several levels of uncertainty and alternatives, making the decision tree representation more complex. Influence

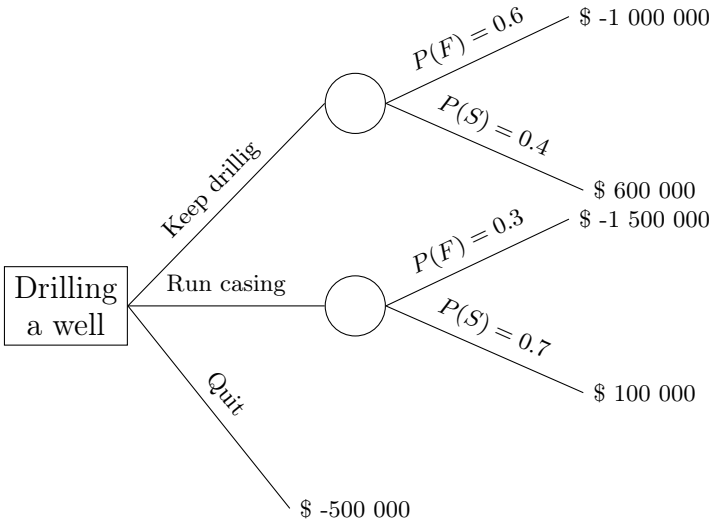

Figure 9: Decision tree for a drilling situation. The alternatives are: keep drilling, run casing, and quit. $P(F)$ is the probability of wellbore failure and $P(S)$ is the probability to successfully reach the reservoir. The leaves are the profits.

diagrams are also a useful way to represent uncertainties and decision relationships (Howard and Matheson, 2005).

Decision making in the oil and gas industry means dealing with uncertainties, given the difficulty to observe directly the conditions in the subsurface, and when measurements are available the data often come with noise. It is of great importance for the decision maker to be able to gather information and improve the uncertainty quantification about the variable of interest before making any decision. Information anyway comes with a cost, it is then vital to carefully evaluate what information is really necessary. While providing the decision maker with opportunities, this also increases the complexities, adding to the decision of taking an action instead of the others, the choice of what type of data to gather. Value of information (VOI) is a helpful tool that can be used to decide whether to gather information or not (Eidsvik et al., 2015). When values are given in monetary unit the VOI is the amount of money that the

decision maker should be willing to spend to acquire the information.

First, let us introduce some mathematical notation and terms before going into the details of VOI. Define $\mathcal{A} = \{a_1, \ldots, a_n\}$ as the set of alternatives and $\boldsymbol{x}$ as the uncertain variable of interest. We define $\nu(\boldsymbol{x}, a)$ as the value function that depends on uncertainty $\boldsymbol{x}$ and alternative a. The decision maker aims to choose the alternative that maximizes the expected value of ν.

When studying the VOI it is important to have in mind the data gathering scheme we are going to adopt and the type of information we are going to acquire. The principal distinction for data gathering is between static and sequential data gathering scheme. A static data gathering scheme consists in obtaining information at the same time, while a sequential data gathering scheme allows us to first gather some information and then based on what has been observed decide if to proceed with more information (Eidsvik et al., 2018). In a similar way one could consider static or sequential decision situation, where one can either take decision in one time, or sequentially, based on the outcome of the previous one. A sequential scheme is more computational demanding and for large problems it requires the application of dynamic programming techniques (Alyaev et al., 2019). The type of information can be divided in perfect or imperfect information. Perfect information consists of measurements not affected by errors, imperfect information on the other hand regards measurements with errors. It is important to stress that VOI analysis is done before the data acquisition actually starts, so we are still uncertain about the outcome of the experiments. We are interested in choosing the information with the largest average value. We will consider a situation of risk neutral decision maker, with a static data gathering scheme.

VOI is computed comparing the posterior value of the information (PoV) when the variable to observe has been chosen, and the prior value (PV), based on the prior belief and knowledge of the decision maker. This can mathematically be expressed for a situation with imperfect information ($\boldsymbol{d}$) with

$$\mathrm{PV} = \max_{a \in \mathcal{A}} \left[\mathbb{E}\left(\nu(\boldsymbol{x}, a)\right) \right], \tag{24}$$

$$\mathrm{PoV}(\boldsymbol{d}) = \int \max_{a \in \mathcal{A}} \left[\mathbb{E}\left(\nu(\boldsymbol{x}, a) | \boldsymbol{d}\right) \right] p(\boldsymbol{d}) \mathrm{d}\boldsymbol{d}. \tag{25}$$

By taking the difference between the posterior and the prior value we obtain the VOI

$$\mathrm{VOI} = \mathrm{PoV}(\boldsymbol{d}) - \mathrm{PV}. \tag{26}$$

Finally, the VOI has to be compared with the cost of data gathering

($C(\boldsymbol{d})$), and the information should be acquired only if $VOI - C(\boldsymbol{d})$ is greater than 0.

The computations of equation (25) can be cumbersome, having to compute two expected values. They can sometimes be simplified in the case of Gaussian distributions, where a close formula is available, or in case of Poisson likelihood where it can be computed with Laplace approximations (Evangelou and Eidsvik, 2017).

Selection of designs

The selection of the optimal design for statistical models can have a great impact on the outcome of the experiment and on its cost. In this section we introduce some of the most common criteria for optimality, with the aim of giving an understanding of the problem.

In our case we use VOI as an design criterion. The reason it is used, is that the decision situation can be rather clearly stated in our application. Moreover, the monetary values associated with outcomes and alternatives can also be specified within reasonable margins. Alternatively, in a situation where no clear decision situations or monetary values are available one could aim to select the best space filling design. In this framework one could, for example choose the design that maximizes the entropy (Nowak and Guthke, 2016; Santner et al., 2003), optimizing the amount of the information contained in the design; or could use Latin Hypercube designs (Pistone and Vicario, 2010; Jourdan and Franco, 2010).

There exist a number of different categories of optimal designs depending on what we aim to maximize or minimize in a more model based statistical setting. The most common optimality criteria are then A-optimality and D-optimality (Shah and Sinha, 2012). In A-optimality the goal is to minimize the trace of the inverse of the covariance matrix of the parameter estimates, while with D-optimality the goal is to minimize the determinant of the same matrix. Finding the optimal design is hence an optimization problem.

No matter what utility functions are used, the computational problem of finding the best design remains. Several methods for finding the optimal design have been developed during the years. García-Ródenas et al. (2020) give an interesting review of some of the main algorithms for the selection of the optimal design, comparing deterministic and metaheuristic approaches. Sequential selection algorithms have been proven to converge for D-optimality (Wynn, 1970). These type of algorithms sequentially add to the starting set points that increase the value of the function we want optimize (Robertazzi and Schwartz, 1989). Exchange algorithms can be used for selection of design as well. Miller and Nguyen

(1994) apply the exchange algorithm to find the D-optimal design. Here, starting from a given design it is possible to exchange the point in the design that is considered to not reduce the value, with the one that is considered to increase the value of the design.

In our settings finding the optimal design corresponds to select the best configurations for data gathering. In geostatistics this will often lead in situations of spatially distributed data.

4 Summary of the papers

The main objective of the thesis is to deliver methodologies and algorithms that can improve the safety of drilling operations and at the same time reduce the cost. The algorithms developed are case based for the fields in the North Sea, but the statistical structure and the methodology have a high level of flexibility and they can be used in a wide range of disciplines.

A summary of the papers is provided, underlying their main contributions and discussing possible future works. The work carried out in the papers has been presented in several international conferences and workshops.

Paper 1: Statistical modeling for real-time pore pressure prediction from predrill analysis and well logs

Jacopo Paglia, Jo Eidsvik, Arnt Grøver, Ane Elisabet Lothe
Published in Geophysics

We study the problem of pore pressure estimation in overpressured layers in an oil and gas field in the North Sea. Accurate pore pressure prediction reduce the risk of drilling accidents, helping to choose the appropriate mud pressure. Unexpected overpressured formations represent one of the biggest risks of fluid influx during drilling. Fluid influx can lead to blowout, creating large environmental and safety issues. The objective is to reduce the prior uncertainty in pore pressure in real time, assimilating new measurements when they get available while drilling. Predrill understanding about pore pressure is available from a 3D geological model. The model takes into account the major mechanisms of pressure generation and dissipation over geologic time in a sedimentary basin. We use the value of pore pressure at present time. A Gaussian process is trained from this geological model data and used as the prior model, taking into account trends and spatial dependencies in pore pressure. The spatial modeling of pore pressure allows data from a given well location to be also informative for other locations in the field. A statistical rock physics

model is used to relate pore pressure with available well logs (resistivity, porosity, and sonic transit time). The likelihood is assumed to be Gaussian, where the expected value is given by the non-linear rock physics relations (Zhang, 2011). A sequential data assimilation method is used to update the pore pressure distribution in real time, when data become available. The approach is based on linearization of the rock physics relation, and it is not dissimilar to a spatial version of the extended Kalman filter. For the situation with a Gaussian prior and a linearized Gaussian likelihood model, the sequential updating of data leads to a posterior Gaussian distribution. The results on the North Sea data show a reduction on the uncertainty of pore pressure as more data are collected.

The main contribution of the paper is a new method for reducing the uncertainty in pore pressure in real time while drilling. The combination of data assimilation and spatial statistical modeling allow uncertainty quantification not only at a given location, but in an area around the data acquisition point. A better understanding of pore pressure will improve the safety of drilling operations and could have large economical benefits for the operating company.

The model is built for a field in the North Sea, but despite the fact of being case specific, it can be applied in other contexts. Other types of measurements can be included in the study, provided with the adequate likelihood functions. Other rock physical relations than the ones used can also be adopted, to adapt the problem to other types of rock formations. The method is based on modeling pore pressure with a Gaussian process. It is possible to extend this work considering instead several realization from Pressim and using a modified version of the ensemble Kalman filter.

The work has been presented at the annual DrillWell conference, Stavanger (Norway); EAGE Conference & Exhibiton, Copenhagen (Denmark); Hawassa Math&Stat Conference, Hawassa (Ethiopia). The work has also been presented in seminars at the Department of Mathematical Sciences at NTNU and in meetings with the companies part of the consortium.

Paper 2: Uncertainties in mud-weight window for safe drilling operations

Jacopo Paglia, Jo Eidsvik, Pierre Cerasi
Under revision in SPE Journal

An accurate MWW helps avoiding well instabilities and damages of the drilling tools. We focus on the uncertainties involved in the MWW, studying how acquisition of new measurements can improve the selection of the adequate mud density. We study a drilling situation in the Norwegian

sector of the North Sea. The workflow presented here has the objective of helping the decision maker in choosing what measurements should be acquired to decide if it is safe enough to keep drilling or if it is necessary to run casing. The realizations of the main parameters needed for the computation of the MWW come from a predrill 3D geologic model of the field. A software that analyzes well instabilities in shale is then used to obtain realizations of MWW from the input parameters. The attention is on the lower limit of the MWW, since companies often choose to use the minimum horizontal stress as upper limit of MWW, taking into consideration that natural fractures may be encountered during drilling. Additionally, being able to drill with low mud pressure can significantly improve the rate of penetration reducing drilling cost. Sensitivity analysis is used to detect the most relevant parameters, based on their main effect and on the interactions. We used a distance based generalized sensitivity analysis (Fenwick et al., 2014) for this purpose, finding out that pore pressure, minimum horizontal stress and unconfined compressive strength are the main parameters. Building on this insight, a statistical model is fitted for the lower limit of the MWW and the main input parameters, keeping in mind their geostatistical trends and dependencies. Finally, VOI analysis is used to determine the best combination of data for making conscious decision on whether keep drilling or set casing.

The new contribution of the paper is to combine sensitivity analysis on the lower limit of the MWW and VOI to select the appropriate combination of data to help the decision maker in carefully deciding on whether to keep drilling or set casing.

The work can be extended to other drilling contexts considering other types of rock formation instead of shale. We can also include other well orientations, or consider situations of stress anisotropy. Additionally, it would be possible to study the upper limit of the MWW for situations where the drilling mud is at a pressure close to the fracturing pressure. During the study we focus on the geomechanical properties of the shale. Chemical and thermal properties could be included as well for sensitivity analysis, given a proper set of input prior realizations.

The work has been presented at SIAM Conference on Mathematical & Computational Issues in the Geosciences (GS19), Houston (USA); Fourth EAGE Conference on Petroleum Geostatistics, Florence (Italy). The work has also been presented in seminars at the Department of Mathematical Sciences at NTNU and in meetings with the companies part of the consortium.

Paper 3: Efficient spatial designs using Hausdorff distance and Bayesian optimization

Jacopo Paglia, Jo Eidsvik, Juha Karvanen

Submitted to Scandinavian Journal of Statistics

We develop a methodology for sequential Bayesian optimization for spatially distributed experimental designs. The work is motivated by earth science problems. In particular from decision situations in the oil and gas industry and in forestry conservation. The goal is to help the decision maker in choosing the optimal combination of spatially distributed information. The decision value function is modeled with a Gaussian process, enabling faster approximations in the iterations of sequential Bayesian optimization. The Hausdorff distance is used to model the dissimilarities between the designs, since it represents the distance between two sets. Expected improvement is the acquisition function that constitute the central part of the iterative Bayesian optimization letting us evaluate the rather expensive VOI only for the most promising designs. A synthetic case is presented, where we can compare the results from the algorithm with the available exact solution. We restart the algorithm 10 times, noticing that it often returns designs with very large values of VOI, and often the resulting design coincides with the optimal one. We compare the algorithm with other approaches such as sequential selection and exchange algorithm. The sequential algorithm seems to be relatively fast, but struggling to get large values of VOI. The exchange algorithm on the other hand returns the design with the largest VOI, but using more evaluations than the ones needed for the algorithm we developed. In the forestry and petroleum applications, we discuss the results obtained by the algorithm and compare it with others. Overall the suggested methodology allows an efficient selection of design with large VOI.

The study deals with the choice of the optimal design among a large set of possible alternative. The main contribution of the work is to introduce the Hausdorff distance to model similarities between designs. Combined with an iterative Bayesian optimization, this allow us to find efficient designs with large VOI.

The study can be extended to more complex probability distributions for data, making it more challenging to compute the VOI. Other applications are also possible in the context of epidemiology for example, or machine learning, opening up for other distances instead of the Hausdorff distance.

The work has been presented in seminars at the Department of Mathematical Sciences at NTNU.

Bibliography

Adams, N. J. and Adams, N. (1985). *Drilling engineering: a complete well planning approach*. Pennwell Corporation.

Addis, M., Hanssen, T., Yassir, N., Willoughby, D., Enever, J., et al. (1998). A comparison of leak-off test and extended leak-off test data for stress estimation. In *SPE/ISRM Rock Mechanics in Petroleum Engineering*. Society of Petroleum Engineers.

Alyaev, S., Suter, E., Bratvold, R. B., Hong, A., Luo, X., and Fossum, K. (2019). A decision support system for multi-target geosteering. *Journal of Petroleum Science and Engineering*, 183:106381.

Asch, M., Bocquet, M., and Nodet, M. (2016). *Data assimilation: methods, algorithms, and applications*, volume 11. SIAM.

Aslannezhad, M., Khaksar manshad, A., and Jalalifar, H. (2016). Determination of a safe mud window and analysis of wellbore stability to minimize drilling challenges and non-productive time. *Journal of Petroleum Exploration and Production Technology*, 6(3):493–503.

Borge, H. (2000). *Fault controlled pressure modelling in sedimentary basins*. PhD thesis, Norwegian University of Science and Technology.

Bowers, G. L. et al. (1995). Pore pressure estimation from velocity data: Accounting for overpressure mechanisms besides undercompaction. *SPE Drilling & Completion*, 10(02):89–95.

Brahma, J., Sircar, A., and Karmakar, G. (2013). Pre-drill pore pressure prediction using seismic velocities data on flank and synclinal part of Atharamura anticline in the Eastern Tripura, India. *Journal of Petroleum Exploration and Production Technology*, 3(2):93–103.

Bratvold, R. and Begg, S. (2010). *Making good decisions*. Society of Petroleum Engineers.

Campolongo, F., Cariboni, J., and Saltelli, A. (2007). An effective screening design for sensitivity analysis of large models. *Environmental modelling & software*, 22(10):1509–1518.

Chen, G., Chenevert, M. E., Sharma, M. M., and Yu, M. (2003). A study of wellbore stability in shales including poroelastic, chemical, and thermal effects. *Journal of Petroleum Science and Engineering*, 38(3):167 – 176. Borehole Stability.

Eaton, B. A. et al. (1975). The equation for geopressure prediction from well logs. In *Fall meeting of the Society of Petroleum Engineers of AIME*. Society of Petroleum Engineers.

Eidsvik, J., Martinelli, G., and Bhattacharjya, D. (2018). Sequential information gathering schemes for spatial risk and decision analysis applications. *Stochastic environmental research and risk assessment*, 32(4):1163–1177.

Eidsvik, J., Mukerji, T., and Bhattacharjya, D. (2015). *Value of information in the earth sciences: Integrating spatial modeling and decision analysis*. Cambridge University Press.

El-Werr, A., Shebl, A., El-Rawy, A., and Al-Gundor, N. (2017). Pre-drill pore pressure prediction using seismic velocities for prospect areas at Beni Suef oil field, Western Desert, Egypt. *Journal of Petroleum Exploration and Production Technology*, 7(4):1011–1021.

Ellis, D. V. and Singer, J. M. (2007). *Well logging for earth scientists*, volume 692. Springer.

Evangelou, E. and Eidsvik, J. (2017). The value of information for correlated GLMs. *Journal of Statistical Planning and Inference*, 180:30 – 48.

Evenick, J. (2008). *Introduction to well logs and subsurface maps*. PennWell Books.

Evensen, G. (2009). *Data assimilation: the ensemble Kalman filter*. Springer Science & Business Media.

Fenwick, D., Scheidt, C., and Caers, J. (2014). Quantifying asymmetric parameter interactions in sensitivity analysis: application to reservoir modeling. *Mathematical Geosciences*, 46(4):493–511.

Fjar, E., Holt, R. M., Raaen, A., Risnes, R., and Horsrud, P. (2008). *Petroleum related rock mechanics*, volume 53. Elsevier.

Fletcher, S. J. (2017). *Data assimilation for the geosciences: From theory to application*. Elsevier.

Fruth, J., Roustant, O., and Kuhnt, S. (2015). Sequential designs for sensitivity analysis of functional inputs in computer experiments. *Reliability Engineering & System Safety*, 134:260–267.

García-Ródenas, R., García-García, J. C., López-Fidalgo, J., Martín-Baos, J. Á., and Wong, W. K. (2020). A comparison of general-purpose optimization algorithms for finding optimal approximate experimental designs. *Computational Statistics & Data Analysis*, 144:106844.

Gramacy, R. B. (2020). *Surrogates: Gaussian Process Modeling, Design, and Optimization for the Applied Sciences*. CRC Press.

Hareland, G., Nygaard, R., et al. (2007). Calculating unconfined rock strength from drilling data. In *1st Canada-US Rock Mechanics Symposium*. American Rock Mechanics Association.

Hassanvand, M., Moradi, S., Fattahi, M., Zargar, G., and Kamari, M. (2018). Estimation of rock uniaxial compressive strength for an Iranian carbonate oil reservoir: Modeling vs. artificial neural network application. *Petroleum Research*, 3(4):336–345.

Howard, R. A. and Matheson, J. E. (2005). Influence diagrams. *Decision Analysis*, 2(3):127–143.

Iooss, B. and Lemaître, P. (2015). A review on global sensitivity analysis methods. In *Uncertainty management in simulation-optimization of complex systems*, pages 101–122. Springer.

Iooss, B. and Prieur, C. (2017). Shapley effects for sensitivity analysis with dependent inputs: comparisons with Sobol'indices, numerical estimation and applications. *arXiv preprint arXiv:1707.01334*.

Jourdan, A. and Franco, J. (2010). Optimal Latin hypercube designs for the Kullback–Leibler criterion. *AStA Advances in Statistical Analysis*, 94(4):341–351.

Julier, S. J. and Uhlmann, J. K. (2004). Unscented filtering and nonlinear estimation. *Proceedings of the IEEE*, 92(3):401–422.

Kalman, R. E. (1960). A new approach to linear filtering and prediction problems. *Journal of basic Engineering*, 82(1):35–45.

Labuz, J. F. and Zang, A. (2012). Mohr–coulomb failure criterion. *Rock mechanics and rock engineering*, 45(6):975–979.

Lahoz, B. K. W. and Menard, R. (2010). *Data assimilation*. Springer.

Lothe, A., Borge, H., and Gabrielsen, R. (2004). Modelling of hydraulic leakage by pressure and stress simulations and implications for Biot's constant: an example from the Halten Terrace, offshore Mid-Norway. *Petroleum Geoscience*, 10(3):199–213.

Lothe, A., Grover, A., Roli, O., Leirdal, G., and Kristiansen, T. G. (2019). Uncertainty modelling of minimum horizontal stresses and porepressures in deeply buried Grabens. What's next in modelling? In *Second EAGE Workshop on Pore Pressure Prediction*.

Mara, T. A. and Tarantola, S. (2012). Variance-based sensitivity indices for models with dependent inputs. *Reliability Engineering & System Safety*, 107:115–121.

Matheron, G. (1963). Principles of geostatistics. *Economic Geology*, 58(8):1246–1266.

Mavko, G., Mukerji, T., and Dvorkin, J. (2020). *The rock physics handbook*. Cambridge university press.

Miller, A. J. and Nguyen, N.-K. (1994). Algorithm AS 295: A Fedorov exchange algorithm for D-optimal design. *Journal of the Royal Statistical Society. Series C (Applied Statistics)*, 43(4):669–677.

Morris, M. D. (1991). Factorial sampling plans for preliminary computational experiments. *Technometrics*, 33(2):161–174.

Myrseth, I. and Omre, H. (2010). *The Ensemble Kalman Filter and Related Filters*, chapter 11, pages 217–246. John Wiley & Sons, Ltd.

Nowak, W. and Guthke, A. (2016). Entropy-based experimental design for optimal model discrimination in the geosciences. *Entropy*, 18(11):409.

Oliver, M. and Webster, R. (2014). A tutorial guide to geostatistics: Computing and modelling variograms and kriging. *Catena*, 113:56–69.

Oyler, D. C., Mark, C., and Molinda, G. M. (2010). In situ estimation of roof rock strength using sonic logging. *International Journal of Coal Geology*, 83(4):484–490.

Park, J., Yang, G., Satija, A., Scheidt, C., and Caers, J. (2016). Dgsa: A matlab toolbox for distance-based generalized sensitivity analysis of geoscientific computer experiments. *Computers & Geosciences*, 97:15–29.

Pistone, G. and Vicario, G. (2010). Comparing and generating Latin Hypercube designs in Kriging models. *AStA Advances in Statistical Analysis*, 94(4):353–366.

Rezaee, R. (2015). *Fundamentals of gas shale reservoirs*. John Wiley & Sons.

Robertazzi, T. and Schwartz, S. (1989). An accelerated sequential algorithm for producing D-optimal designs. *SIAM Journal on Scientific and Statistical Computing*, 10(2):341–358.

Rommetveit, R., Bjorkevoll, K. S., Cerasi, P. R., Havardstein, S. T., Fjeldheim, M., Helset, H. M., Odegard, S. I., and Nordstrand, C. (2010). Real time integration of ECD, temperature, well stability and geo/pore pressure simulations during drilling a challenging HPHT well. In *SPE Intelligent Energy Conference and Exhibition*. Society of Petroleum Engineers.

Rousseeuw, P. J. (1987). Silhouettes: a graphical aid to the interpretation and validation of cluster analysis. *Journal of computational and applied mathematics*, 20:53–65.

Sacks, J., Welch, W. J., Mitchell, T. J., and Wynn, H. P. (1989). Design and analysis of computer experiments. *Statistical science*, 4(4):409–423.

Saltelli, A., Annoni, P., Azzini, I., Campolongo, F., Ratto, M., and Tarantola, S. (2010). Variance based sensitivity analysis of model output. Design and estimator for the total sensitivity index. *Computer Physics Communications*, 181(2):259–270.

Saltelli, A., Ratto, M., Andres, T., Campolongo, F., Cariboni, J., Gatelli, D., Saisana, M., and Tarantola, S. (2008). *Global sensitivity analysis: the primer*. John Wiley & Sons.

Santner, T. J., Williams, B. J., Notz, W., and Williams, B. J. (2003). *The design and analysis of computer experiments*, volume 1. Springer.

Särkkä, S. (2013). *Bayesian filtering and smoothing*, volume 3. Cambridge University Press.

selmandesign.com (2017). selmandesign. `https://www.autodraw.com`. Accessed January 2019.

Shah, K. R. and Sinha, B. (2012). *Theory of optimal designs*, volume 54. Springer Science & Business Media.

Sobol, I. M. (1993). Sensitivity estimates for nonlinear mathematical models. *Mathematical modelling and computational experiments*, 1(4):407–414.

Sobol, I. M. (2001). Global sensitivity indices for nonlinear mathematical models and their Monte Carlo estimates. *Mathematics and computers in simulation*, 55(1-3):271–280.

Stassi-D'Alia, F. (1967). Flow and fracture of materials according to a new limiting condition of yelding. *Meccanica*, 2(3):178–195.

Su, G., Peng, L., and Hu, L. (2017). A Gaussian process-based dynamic surrogate model for complex engineering structural reliability analysis. *Structural Safety*, 68:97–109.

Torsæter, M. and Cerasi, P. (2015). Mud-weight control during arctic drilling operations. In *OTC Arctic Technology Conference*. Offshore Technology Conference.

Ulusay, R. (2014). *The ISRM suggested methods for rock characterization, testing and monitoring: 2007-2014*. Springer.

Wynn, H. P. (1970). The sequential generation of D-optimum experimental designs. *The Annals of Mathematical Statistics*, pages 1655–1664.

Zendehboudi, S. and Bahadori, A. (2016). *Shale oil and gas handbook: theory, technologies, and challenges*. Gulf Professional Publishing.

Zhang, J. (2011). Pore pressure prediction from well logs: Methods, modifications, and new approaches. *Earth-Science Reviews*, 108(1-2):50–63.

Zoback, M. D. (2010). *Reservoir geomechanics*. Cambridge University Press.

Statistical modeling for real-time pore pressure prediction from predrill analysis and well logs

Jacopo Paglia, Jo Eidsvik, Arnt Grøver, Ane Elisabet Lothe

Published in Geophysics

GEOPHYSICS, VOL. 84, NO. 2 (MARCH-APRIL 2019); P. ID1–ID12, 13 FIGS., 4 TABLES.
10.1190/GEO2018-0168.1

Statistical modeling for real-time pore pressure prediction from predrill analysis and well logs

Jacopo Paglia[1], Jo Eidsvik[1], Arnt Grøver[2], and Ane Elisabet Lothe[2]

ABSTRACT

The challenge of pore pressure prediction in an overpressured area near a well is studied. Predrill understanding of pore pressure is available from a 3D geologic model for pressure buildup and release using a basin modeling approach. The pore pressure distribution is updated when well logs are gathered while drilling. Sequential Bayesian methods are used to conduct real-time pore pressure prediction, meaning that every time new well logs are available, the pore pressure distribution is automatically updated ahead of the bit and in every spatial direction (north, east, and depth), with associated uncertainty quantification. Spatial modeling of pore pressure variables means that the data at one well depth location will also be informative of the pore pressure variables at other depths and lateral locations. A workflow is exemplified using real data. The prior model is based on a Gaussian process fitted from geologic modeling of this field, whereas the likelihood model of well-log data is assessed from data in an exploration well in the same area. Results are presented by replaying a drilling situation in this context.

INTRODUCTION

Prediction of abnormal pore pressure is an important part of subsurface modeling. It is controlled by pressure generating and dissipating geologic processes that have taken place over millions of years. It is also determined by the fault pattern and how a sedimentary basin with pressure compartments has been formed over years. This process is essential for understanding current-day pore pressure distributions, which are important in exploration and development drilling operations. Accurate pore pressure prediction helps avoid drilling risks because it allows improved tuning of the mud weights and one can reduce drilling costs by wisely choosing the casing point before entering the reservoir or some high-pressure formation, see, e.g., Rommetveit et al. (2010) or Gholami et al. (2015).

The focus of this paper is pore pressure prediction from predrill assessments and well-log measurements. We present a new approach for real-time prediction of pore pressure, using the predrill assessment as a prior distribution, and updating the distribution when new measurements become available while drilling. First, a basin modeling approach, building on interpreted seismic horizons, and 3D pressure modeling is used for predrill evaluation. Then, the pore pressure distribution ahead of the bit and at other lateral and depth locations is updated by integrating well-log information while drilling. This modeling approach is connected to a system or workflow for automized updating of pore pressure, which is important for improved decision making. Note that seismic velocities could also be used for predrill assessment of pore pressure (Dutta, 2002; Sayers et al., 2002; Chopra and Huffman, 2006; Ugwu, 2015). In some depositional systems, such data would give a more refined predrill model, of course at the cost of extracting more information from the data.

There exist several rock-physics models that relate pore pressure to petrophysical or geophysical variables. Eaton's method (Eaton, 1975) is extensively used for pore pressure estimation from resistivity or sonic traveltime data. Bowers (1995) also proposes a method for pore pressure estimation based on velocity data. Zhang (2011) includes a depth-dependent normal compaction trend line in Eaton's methods, developing a new method for pore pressure prediction from porosity. In the current paper, we build on Zhang's equation, and we use data to learn free model parameters within that functional relationship.

Because the predictions of pore pressure are commonly applied to make decisions about the well mud weight and casing points, it is critical to get some realistic level of the uncertainty in the prediction (López et al., 2004; Wessling et al., 2013). We advocate Bayesian modeling, which naturally allows for consistent uncertainty quantification as part of the workflow. Bayesian statistics have been applied to pore pressure prediction previously: Malinverno et al. (2004)

Manuscript received by the Editor 6 March 2018; revised manuscript received 20 September 2018; published ahead of production 03 December 2018; published online 11 February 2019.
[1]NTNU, Department of Mathematical Sciences, Trondheim, Norway. E-mail: jacopo.paglia@ntnu.no; jo.eidsvik@ntnu.no.
[2]SINTEF Industry, Exploration and Reservoir Technology Group, Trondheim, Norway. E-mail: arnt.grover@sintef.no; aneelisabet.lothe@sintef.no.

use a Bayesian method to update pore pressure predictions based on logs and check shot information, with relations provided by Eaton's equations. Bektas et al. (2015) apply a sequential modeling approach to pore pressure prediction. Oughton et al. (2017) use a Bayesian network model to connect the pore pressure variables at different depths, and to different kinds of data. These approaches are similar to what we are doing here, but without the same focus on the spatial modeling aspect and on learning the prior and likelihood models from data. In the current paper, we also conduct a sensitivity analysis to different input parameters in this model and we evaluate the effect of different data on the pore pressure distribution.

The paper is organized as follows. We start with a background description of the main parts required to conduct real-time pore pressure prediction. Then, we outline the prior model, the likelihood fitting, and the sequential updating method for real-time prediction. Results and discussion are based on a real-data case.

PROBLEM DESCRIPTION

The pore pressure is denoted as $\mathbf{p} = (p_1, \ldots, p_n)$, where $p_i = p(\mathbf{s}_i)$ is the pore pressure at spatial location $\mathbf{s}_i = (s_{i1}, s_{i2}, s_{i3})$, represented by the north, east, and depth coordinates, and n is the number of locations. The predrill information about the pore pressure consists of geologic understanding of the sediments based on the interpreted reflection seismic horizons and interpreted faults. The simulated pore pressure in the predrill case is a result of modeling pressure generation and dissipation in 3D over millions of years.

The well-log data are denoted as $\mathbf{y}_j$, where the index j refers to data collected over the well path order $j = 1, \ldots, N$ and N is the total number of data points considered. We can further clarify this by using notation $\mathbf{y}_j(\mathbf{s}_{w,j})$, indicating that the well is at spatial location $\mathbf{s}_{w,j}$ at step j. In our case, we consider resistivity logs (r), neutron porosity (ϕ) and acoustic logs of traveltime (Δt), so that data are $\mathbf{y}_j = (r_j, \phi_j, \Delta t_j)$. Figure 1 illustrates the situation in which the pore pressure variables are represented on a regular 3D grid, and the well trajectory is oriented vertically.

When the drilling operation starts, the goal is to assimilate data in real time. This means that the data $\mathbf{y}_1, \ldots, \mathbf{y}_N$ are assimilated in a sequential manner, and one obtains step-wise updating of the distribution for the pore pressure variables $\mathbf{p}$ at all grid locations.

Our suggested workflow for pore pressure prediction is as follows:

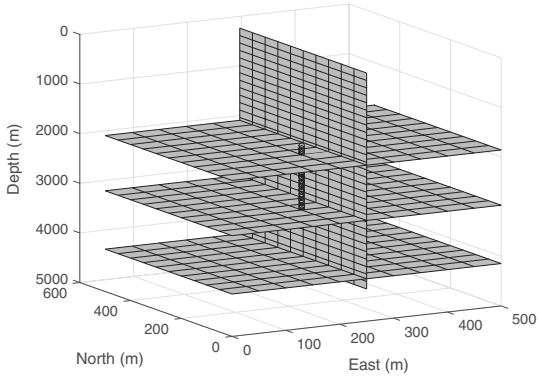

Figure 1. Illustration of slices of a 3D grid covering a subsurface domain. At each site in the grid, we aim to predict the pore pressure. The black points represent the well path where resistivity, neutron porosity, and traveltime log data are gathered.

1) Train a prior distribution from pore pressure variables obtained from geologic modeling.
2) Specify the likelihood model for well-log data based on the available logs in the vicinity of the current location.
3) Use a sequential updating method for real-time pore pressure prediction.

We will go through these steps in the next three sections.

PRIOR MODEL — PREDRILL ASSESSMENT FROM GEOLOGIC MODELING

We construct a multivariate prior distribution for pore pressure variables in the subsurface domain by using extensive predrill assessment based on geologic modeling. In our case, the predrill information is given by Pressim (Borge, 2000; Lothe, 2004), which is software developed by SINTEF Petroleum Research. Pressim is a tool for modeling pressure generation and dissipation within sedimentary basins over geologic time. The modeled pressure generation is controlled by the degree of mechanical and chemical compaction, whereas the pressure dissipation and lateral pressure transfer is controlled by flow barriers such as faults and low permeable sedimentary units such as shales or salt. The pressure generation due to compaction and diagenesis, and dissipation due to hydraulic failure and leakage (Lothe et al., 2004), is calculated from burial and possible uplift in the study area (Lothe and Grøver, 2009). Overall, the modeled present-day pressure distribution within the basin is a result of its burial history.

A sedimentary basin is a dynamic system over geologic time. It may experience periods with rapid burial leading to a high degree of compaction, but also periods with sediment erosion and uplift leading to high degree of pressure dissipation due to fracturing and leakage. The sediment rock physical properties such as permeability, and the sealing properties of the fault zones may accordingly change with time. The change in porosity is in Pressim given by compaction curves (Sclater and Christie, 1980) and kinetic equations reflecting the degree of chemical compaction, such as quartz growth in sandstone reservoir controlled by the temperature (Walderhaug, 1996). The tool quantifies pressure dissipation using a model for lateral cross-fault fluid flow, and Darcy's flow equation in the vertical direction. The sediment permeability is given by Kozeny-Carman equations (Mavko et al., 2009), linked to its lithology and associated calculated porosity. The modified Griffith-Coulomb failure (Jaeger and Cook, 1963) and the frictional-sliding criterion (Twiss and Moores, 1992) are included to simulate hydraulic leakage from overpressured compartments. We get the sand clay fraction from existing well logs, to set up the geomodel. The quality of the modeled pressure distribution is given by the misfit with observed pressure values at existing well locations.

A general pitfall with this basin modeling approach is the large number of input parameters, their inherent uncertainty, as well as the uncertainty of the process model itself. Several inputs may give similar fit to observations. To capture these issues of the complex problem, a Monte Carlo approach is used, in which the input parameters to the geologic model are varied (Lothe and Grøver, 2009). In our setting, we only consider a few Monte Carlo realizations and we only study the pore pressure at the present time.

Figure 2 shows the spatial structure of the field under consideration. Based on the interpreted reflection seismic and interpreted faults, the study area is divided into 18 depth layers of various thick-

ness (Figure 2a) and 41 vertical compartments (Figure 2b). The overburden shales are rather flat in the study area, whereas the reservoir forms a dome structure. The faults have minor throw; see the model description in Lothe et al. (2018). Figure 2b shows color-coded compartments and many other minor faults. Predrill pressure simulations are carried out for the last 34 millions years, using forward modeling with the pressure calculated every 10,000 years.

Figure 3 shows simulated pore pressure as a function of depth for all the compartment locations in the study area, together with the hydrostatic pressure and the overburden stress, which are also given from the predrill model. We notice a trend of increasing pore pressure as a function of depth. The predrill model predicts that pore pressure is close to the hydrostatic pressure (normal pressure, the red line in Figure 3) for the first 1000 m, then we have overpressure (abnormal pressure). The overpressures from 1000 to 3000 m in the shaly overburden are mainly generated by the illite-smectite diagenesis (Lothe et al., 2018). At depths between 3000 and 4000 m, the model predicts a drop in pore pressure that remains well above the hydrostatic pressure. Less than 4000 m there seems to be increased pore pressure, which is closer to the overburden stress (the blue line in Figure 3). The ability of the predrill model to predict pressures correctly has been tested in several different study areas, such as the Halten terrace area (Lothe, 2004) and northern North Sea (Borge, 2000), with positive results.

One reason for conducting real-time pore pressure updating is to make improved decisions related to drilling mud weight in regions where there is overpressure. For the case that we are considering, the mud weight specification is associated with pore pressure relative to the hydrostatic and overburden pressure. It is for this reason natural to build a statistical model in which we avoid values of pore pressure lower than hydrostatic pressure or greater than the overburden stress. Hence, we introduce the following constraints:

$$p_{h_i} < p_i < p_{ob_i} \quad i = 1, \ldots, n, \tag{1}$$

where p_{h_i} represents the fixed hydrostatic pressure and p_{ob_i} is the fixed overburden stress, at (depth of) location $\mathbf{s}_i$. Statistical modeling with constraints can be difficult, and one standard way to go around this is to use another variable $x_i \in (-\infty, \infty)$ defined by a logistic transform (Dobson and Barnett, 2008) as follows:

$$x_i = \log\left(\frac{p_i - p_{h_i}}{p_{ob_i} - p_i}\right) \quad i = 1, \ldots, n. \tag{2}$$

We will base the prior model on this transformed pore pressure variable. The pore pressure p_i at location $\boldsymbol{s}_i$ can be directly computed from x_i by the inverse of equation 2:

$$p_i = \frac{e^{x_i} p_{ob_i} + p_{h_i}}{1 + e^{x_i}} \quad i = 1, \ldots, n. \tag{3}$$

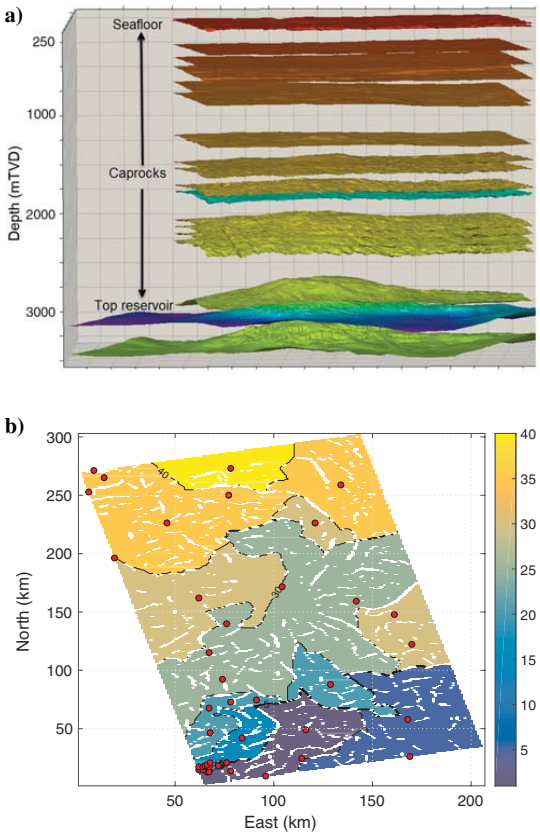

Figure 2. Geometry of the available predrill information. Based on the interpreted seismic horizons used in the Pressim geomodel, the study area is divided in 18 horizontal layers of various thickness and 41 vertical compartments. (a) Vertical view of the field. (b) Map view, the faults only partially seal the compartments. Circles indicate geometric centers of compartments and constitute the sites where prior information were available. The colorbar helps to identify the compartments.

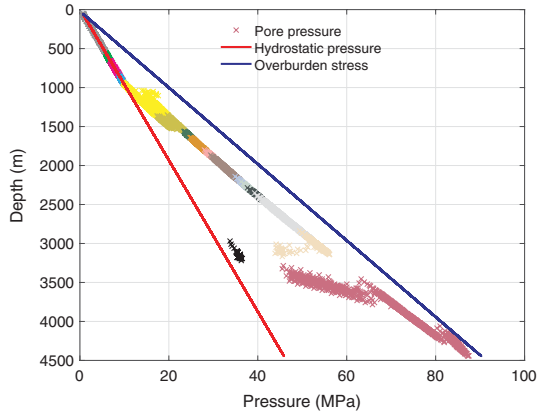

Figure 3. Predrill pore pressure (colored) plotted as a function of depth together with the hydrostatic pressure (red) and the overburden stress (blue) that are also given from the predrill model. The different colors indicate the different layers in which the information about pore pressure is obtained. The model predicts normal pressure for the first 1000 m and then the overpressure starts, and even though there is a drop in the predicted pore pressure between 3000 and 4000 m, the pore pressure remains well above the hydrostatic pressure.

We now build a prior model for the transformed pore pressure at all locations, i.e., $\mathbf{x} = (x_1, \ldots, x_n)$. We construct a multivariate Gaussian distribution in which regression models represent the prior mean as a function of layers and depth, and where variograms are used to study the spatial variability and correlation between the sites of the grid. For each layer k of the overpressured area, focusing then on the deeper layers ($k \geq 6$):

$$x_{i_k,k} = \beta_{0,k} + \beta_{1,k} s_{i_k 3,k} + \epsilon_{i_k,k} \quad k = 6, \ldots, 18, \qquad (4)$$

where $(s_{i_k 3,k}, x_{i_k,k})$ represent the depth and logistic pore pressure defined in equation 2, observed in layer k, and at coordinate $i_k \in I_k = \{1, \ldots, n_k | n_k \text{ number of sites in layer } k\}$. We assume that $\mathbb{E}(\epsilon_{i_k,k}) = 0$ and that the variance is constant, $\mathrm{Var}(\epsilon_{i_k,k}) = \sigma_k^2$ for each $i_k \in I_k$. The estimates of the regression intercept $\beta_{0,k}$ and slope $\beta_{1,k}$ are derived using the method of least squares. We then specify the regression coefficients $\hat{\beta}_{1,k} = \sum_{i_k \in I_k} (x_{i_k,k} - \bar{x}_k)(s_{i_k 3,k} - \bar{s}_{3,k}) / \sum_{i_k \in I_k} (s_{i_k 3,k} - \bar{s}_{3,k})^2$ and $\hat{\beta}_{0,k} = \bar{x}_k - \hat{\beta}_{1,k} \bar{s}_{3,k}$, with $\bar{x}_k$ and $\bar{s}_{3,k}$ sample means within the layer k.

Figure 4 shows the residuals of the regression analysis for layer 8 (there is similar behavior in other layers). Such residual plots are used to check if the model assumptions are fulfilled. In the histogram of the residuals, the frequency of the residual values is plotted. We notice the typical bell shape of the Gaussian distribution, equally distributed at approximately zero, confirming the modeling approach. The other plots are used to check the assumptions of constant variance of the residuals (Figure 4c) and remaining model correlation (Figure 4d).

The spatial covariance is studied further using variograms (Goovaerts, 1997) of the residuals, within the layers and between the layers. Figure 5a and 5b shows the empirical semivariograms together with fitted models.

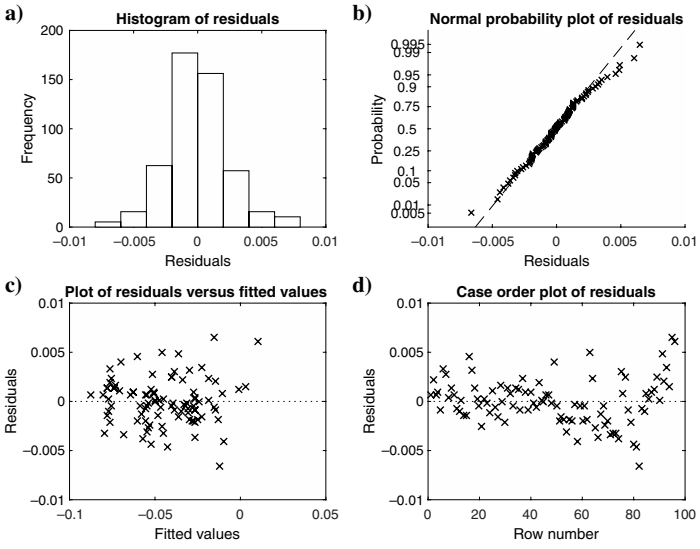

Figure 4. Residuals of the regression analysis for layer 8. (a) The histogram shows the typical symmetric bell shape of the Gaussian distribution, and (b) the normal probability plot further confirms this idea. (c) Residuals versus fitted values check the assumption of constant variance of the residuals, and because they are evenly spread at approximately zero, we can say this is fulfilled. (d) The pattern in the order plot indicates the possible residual correlation in the model.

The fitted variograms are based on the exponential model, in which the lateral and vertical functions are

$$\gamma_k(h) = \sigma_k^2 \left(1 - \exp\left(-\frac{h}{r_k}\right)\right) \quad k = 6, \ldots, 18, \qquad (5)$$

$$\gamma_c(h) = \sigma_c^2 \left(1 - \exp\left(-\frac{h}{r_c}\right)\right) \quad c = 1, \ldots, 41, \qquad (6)$$

where h is the distance between points, r is the range parameter of the variogram, which is indicative of correlation distance, σ_k^2 is the adjusted variance in layer k, and σ_c^2 is the adjusted variance along the compartment c. These σ values correspond to the sill representing the asymptotic level of the variogram for large distance h. Figure 5 shows how the sill value changes if we consider the semivariogram for layer or the one for column; this means that we have a larger variability within the column compared with the layers. Note that the sill value for the semivariogram in layer 8 (Figure 5a) corresponds to the variance of the residual of that layer (Figure 4).

Overall, we build the covariance matrix for the logistic pore pressure variable for any two sites by

$$\Sigma(\mathbf{s}_{i,k}, \mathbf{s}_{j,l}) = \sigma^2 \exp\left(-\frac{\sqrt{(s_{i1,k} - s_{j1,l})^2 + (s_{i2,k} - s_{j2,l})^2}}{r_1} - \frac{|s_{i3,k} - s_{j3,l}|}{r_2}\right), \qquad (7)$$

where $\sigma^2 = 1/13 \sum_{k=6}^{18} \sigma_k^2$ is the average of the standard deviations (SDs) for the layers and r_1 and r_2 are the average range for the variograms per layers and per compartments.

In summary, we then have a prior distribution

$$\pi(\mathbf{x}) = N(\mathbf{x}; \mu, \Sigma), \qquad (8)$$

where $N()$ denotes the multivariate Gaussian density function. The mean $\mu = (\mu_{x_1}, \ldots, \mu_{x_n})$ depends on the fitted regression parameters derived by least squares for equation 4, and the covariance matrix Σ is defined in equation 7.

Recall that the pore pressure p_i is defined from equation 3. Even though we always work with the transformed variable x_i, we plot and interpret results for the pore pressure p_i. The distribution of pore pressure can be approximated using, for instance, a first-order Taylor expansion of equation 3 centered in μ_{x_i}. We then get

$$p_i(x_i) \approx p_i(\mu_{x_i}) + p_i'(\mu_{x_i})(x_i - \mu_{x_i}) \quad i = 1, \ldots, n, \qquad (9)$$

and so

$$\mathbb{E}(p_i) \approx p_i(\mu_{x_i}) \quad i = 1, \ldots, n, \qquad (10)$$

$$\mathrm{Var}(p_i) \approx (p_i'(\mu_{x_i}))^2 \mathrm{Var}(x_i) \quad i = 1, \ldots, n. \tag{11}$$

A similar approach can be used for the multivariate properties of the pore pressure.

In Figure 6, we show the resulting mean and 90% prior prediction interval for the pore pressure, as well as the correlation matrix. This is representative of the 3D grid shown in Figure 1.

The correlation is here organized according to the layers, and we notice great dependence within layers and between sites that are close. When the distance between locations increases, the correlation gets very low.

LIKELIHOOD MODEL — SPECIFICATION FROM WELL-LOG DATA AND PHYSICAL MODELS

The likelihood model should describe the probability distribution of well-log responses as a function of pore pressure. There are several rock-physics relations linking pore pressure to petrophysical and geophysical variables (Mavko et al., 2009). However, they are often complicated by multivariable interactions in the relations, and they tend to work in specific environments, for instance, depending on the compaction as in the Gulf of Mexico (Sayers et al., 2005). It is known that porosity depends on pore pressure, but it also depends on the lithologic composition and other attributes. Therefore, it is difficult to extract pore pressure from porosity unless we know the other variables going into the equation, or know that the study is representative of an area where rapid subsidence and compaction is the main driving mechanism. The same is true for other petrophysical variables. Thus, the specification of a likelihood model would be case specific. We build our likelihood model using the existing relation by Zhang (2011), and we train free model parameters from well-log data. Other models could be equally applicable, but a similar workflow would hold. In the following, we outline the assumptions going into our procedure.

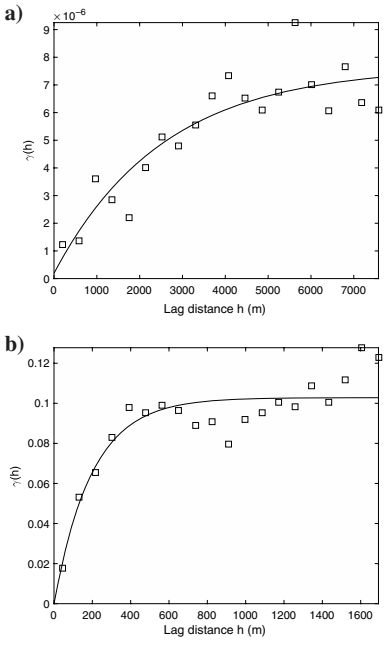

Figure 5. Empirical and fitted exponential semivariograms as function of the lag distance. (a) Layer 8, (b) compartment 41.

The likelihood model is specified from measurements acquired in a well in the same field (the data are provided by ConocoPhillips and the Norwegian Petroleum Directorate). The data consist of logs within a depth domain of the formation. We focus our attention on resistivity, neutron porosity, and sonic logs, as well as gamma ray data.

Figure 7 shows the data as a function of measured depth (MD). We choose to focus on this specific depth interval (3105–3420 m) because it corresponds to an area where all the data are available. We notice that we have much larger resistivity values near 3200 m. This is an oil-saturated zone. Likewise, we have a much larger gamma ray at approximately 3240 m, representing the interval in which we pass from the upper formation to the lower formation.

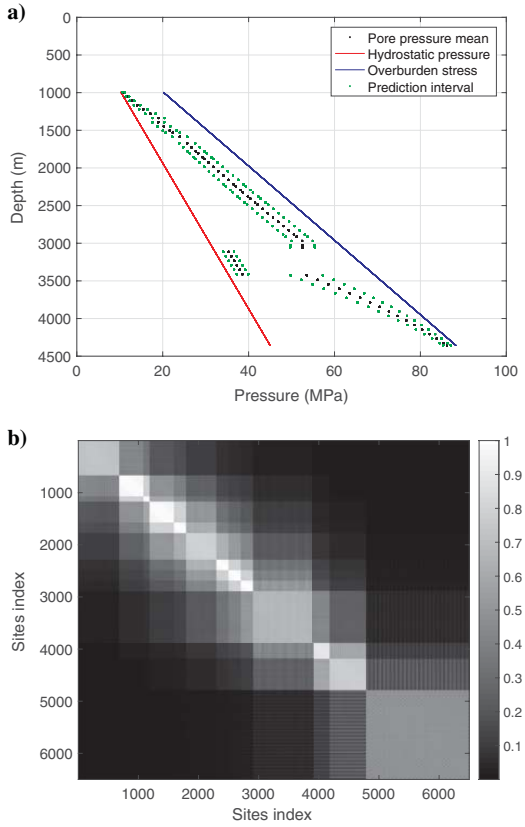

Figure 6. The prior model for pore pressure is a multivariate Gaussian distribution with mean μ and covariance Σ. The dimension is given by the number of sites in the spatial grid. (a) Pore pressure prior mean (black) with a 90% prediction interval (green) together with the hydrostatic pressure and the overburden stress. (b) Prior correlation matrix for pore pressure. It is organized according to the layers, meaning that each site of the grid is sequentially assigned to an index. For close sites the difference of the respective site indexes will be low. The correlation matrix helps to highlight the large correlation within layers and between sites that are close.

We decided to remove these parts (the dashed depth zone in Figure 7) from the data set because they would distract the focus on modeling the pore pressure. This is commonly done in inverse problems because there are many possibilities for getting the same response, and some parameters must be fixed in the modeling, whereas others are treated as random and assigned distributions (Malinverno and Parker, 2006). In the current setting, there are also other inputs, such as temperature and salinity, which influence the response, but they are quite well-known for the North Sea (Bhakta et al., 2016), and not considered in this study.

The likelihood model tying pore pressure to log measurements is here represented by a Gaussian distribution with nonlinear expected values based on rock-physics relations described by Zhang (2011). Given a pore pressure input, the model for resistivity, porosity, and transit time measurements is defined by

$$\mathbf{y}_j = \begin{pmatrix} r_j \\ \phi_j \\ \Delta t_j \end{pmatrix} = \begin{pmatrix} \left(\frac{p_{ob_j}-p_j}{p_{ob_j}-p_{h_j}}\right)^{1/n_r} r_0 e^{bz_j} \\ \phi_0 \exp\left(-\frac{p_{ob_j}-p_j}{p_{ob_j}-p_{h_j}} c_\phi z_j\right) \\ (\Delta t_{ml}-\Delta t_m)\exp\left(\frac{p_j-p_{ob_j}}{p_{ob_j}-p_{h_j}} c_t z_j\right)+\Delta t_m \end{pmatrix} + \begin{pmatrix} \epsilon_{r_j} \\ \epsilon_{\phi_j} \\ \epsilon_{\Delta t_j} \end{pmatrix} \tag{12}$$

$$\Rightarrow \mathbf{y}_j = \mathbf{g}_j(p_j) + \epsilon_j, \quad \epsilon_j \sim N(\mathbf{0}, \mathbf{R}), \quad j = 1, \ldots, N. \tag{13}$$

The 3×1 function $\mathbf{g}(p) = (\mathbb{E}(r|p), \mathbb{E}(\phi|p), \mathbb{E}(\Delta t|p))$ represents the expected values of resistivity, porosity, and transit time, given the pore pressure input, i.e., $\mathbb{E}(\mathbf{y}|p)$. The function $\mathbf{R}$ is the 3×3 measurement noise covariance matrix.

Many parameters in the expectation part of equation 12 must be specified. First, values for p_{ob} and p_h are derived from the Pressim realizations. Moreover, z_j is the depth at measurement location j. For the resistivity function, n_r is the Eaton exponent, r_0 is the normal compaction shale resistivity at the mudline, and b is the slope of logarithmic resistivity normal compaction trendline. For the porosity equation, ϕ_0 is the porosity at the mudline and c_ϕ a constant that can be derived from the normal compaction porosity trendline. Finally, in the sonic transit time function, Δt_{ml} is the compressional transit time in the shale matrix, whereas Δt_m is the mudline transit time and c_t is a constant (Zhang, 2011). These values are chosen based on the parametric form in equation 12 with parameters tuned to fit the well-log data (Table 1).

Figure 8 shows the well logs in gray, the expectation part of the functions in equation 12 in black (where the pore pressure comes from the Pressim realizations). When constructing the expectation part in these plots, we varied pore pressure between the normal pressure and the overburden stress at a depth of 3350 m and evaluated equation 12 for resistivity, porosity, and transit time.

The noise terms ϵ_j in equation 13 are assumed to be independent at different steps j, and this means that the measurements are considered to be only location-wise dependent. Hence, the likelihood model involves conditional independence such that

$$\pi(\mathbf{y}|\mathbf{x}) = \prod_j^N \pi(\mathbf{y}_j|\mathbf{x}) = \prod_j^N \pi(\mathbf{y}_j|x_j), \tag{14}$$

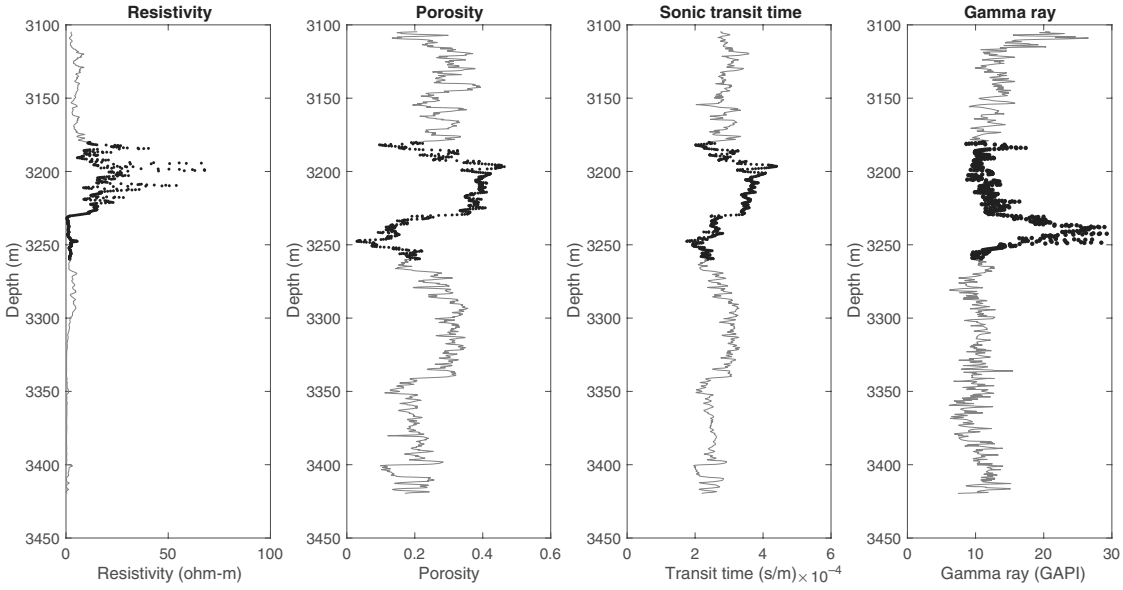

Figure 7. Well-log measurements of resistivity, neutron porosity, sonic transit time, and gamma ray as functions of the MD. In the likelihood fitting, the dashed black parts are ignored because they would distract the focus on modeling the pore pressure. The depth interval considered here goes from 3105 to 3420 m, and it corresponds to an area where all the data are available.

where, in short, $x_j = x(\mathbf{s}_{w,j})$ is the logistic pore pressure at well-log location j. From equation 13, we have

$$\pi(\mathbf{y}_j|x_j) = N(\mathbf{y}_j; \mathbf{g}_j(p_j), \mathbf{R}), p_j = p(x_j). \quad (15)$$

We assume that the error covariance matrix $\mathbf{R}$ is constant over the time steps. We next specify this covariance matrix from residual variability in the data and the rock-physics models.

Using a first-order Taylor expansion centered in μ_j, we get

$$\mathbf{g}_j(p_j) \approx \mathbf{g}_j(\mu_j) + \frac{\partial \mathbf{g}_j}{\partial p_j}|_{\mu_j}(p_j - \mu_j) \quad j = 1, \ldots, N; \quad (16)$$

Hence,

$$\mathbb{E}(\mathbf{y}_j) = \mathbf{g}_j(\mu_j) \quad j = 1, \ldots, N, \quad (17)$$

$$\mathrm{Var}(\mathbf{y}_j) = \mathbf{R} + \frac{\partial \mathbf{g}_j}{\partial p_j}\Big|_{\boldsymbol{\mu}_j} \mathrm{Var}(p_j) \frac{\partial \mathbf{g}_j}{\partial p_j}\Big|_{\boldsymbol{\mu}_j}^t \quad j = 1, \ldots, N. \quad (18)$$

From equation 18, we then obtain an estimate for the covariance $\mathbf{R}$

$$\hat{\mathbf{R}} = \frac{\sum_{j=1}^{N}(\mathbf{y}_j - \mathbf{g}_j(\mu_j))(\mathbf{y}_j - \mathbf{g}_j(\mu_i))^t}{N} - \frac{\partial \mathbf{g}_j}{\partial p_j}\Big|_{\boldsymbol{\mu}_j} \mathrm{Var}(p_j) \frac{\partial \mathbf{g}_j}{\partial p_j}\Big|_{\boldsymbol{\mu}_j}^t. \quad (19)$$

Here, the variance $\mathrm{Var}(p_j)$ is constant because all the well-log sites belong to the same layer.

Applying the previous calculation to the data, we get

$$\hat{\mathbf{R}} = \begin{pmatrix} 6.8137 & 0.1503 & 8.5835 \times 10^{-5} \\ 0.1503 & 0.0083 & 4.4036 \times 10^{-6} \\ 8.5835 \times 10^{-5} & 4.4036 \times 10^{-6} & 2.5930 \times 10^{-9} \end{pmatrix}. \quad (20)$$

We see that there is some correlation in the data, in particular between resistivity and porosity. Not only do the variances indicate measurement errors, but they are also a result of how well the equations in our model fit the data. The resistivity error is very large, compared with that of porosity and sonic transit time. This is also clear from Figure 9, in which the center lines show the likelihood functions in equation 12 plotted as a function of pore pressure

Table 1. Parameter values for equation 12.

Parameter values		
Resistivity	Porosity	Transit time
$n_r = 1.2$	$\phi_0 = 0.574$	$\Delta t_{ml} = 0.65 \times 10^{-3}$ s/m
$r_0 = 0.43$ ohm-m	$c_\phi = 0.39 \times 10^{-3}$ m^{-1}	$\Delta t_m = 0.20 \times 10^{-3}$ s/m
$b = 0.12 \times 10^{-4}$	—	$c_t = 0.9 \times 10^{-3}$ m^{-1}

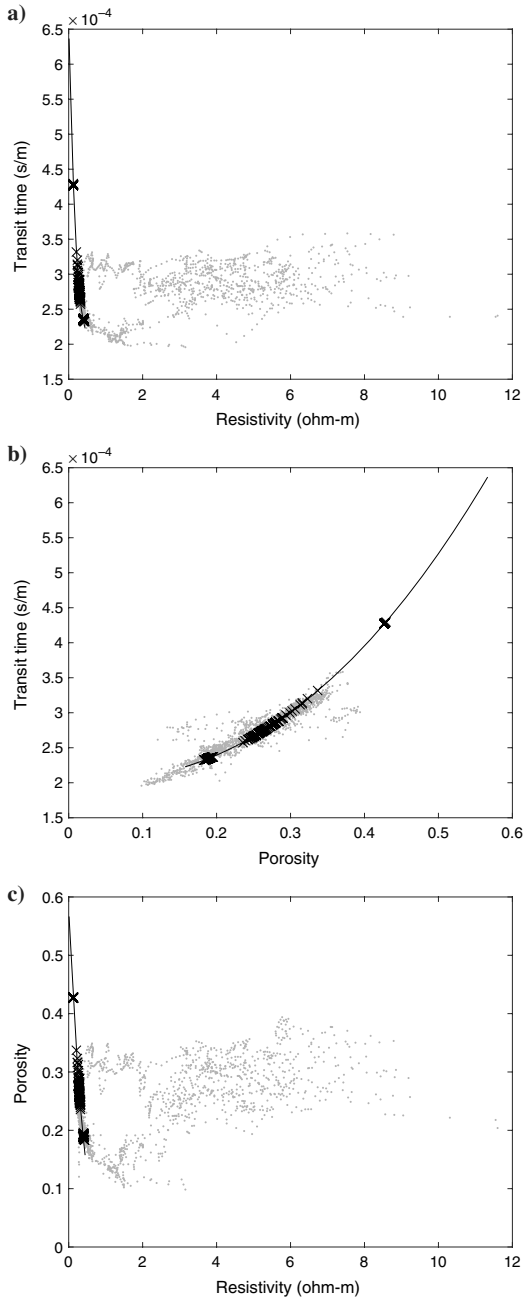

Figure 8. Crossplots of the well-log data (dots) and the expected value in the likelihood (black is the functional link, and the cross is this function evaluated at pressure outputs around the same depth with Pressim output).

varying between the hydrostatic pressure and the overburden stress at a given depth of 3350 m.

It appears as if the porosity and transit time are relatively accurate, based on our model errors, and these data should likely provide useful information about the pore pressure variables in our situation.

SEQUENTIAL UPDATING

The Bayesian formalism, with a prior model for pore pressure variables and likelihood models for the data, is suitable for consistent assimilation of multiple data sources. In our case, the goal is to perform real-time updating of the pore pressure, at any location, when data are acquired in the well. This means that we include well-log data in a step-wise manner while drilling, and the posterior after one update becomes the prior for the next step, and so on.

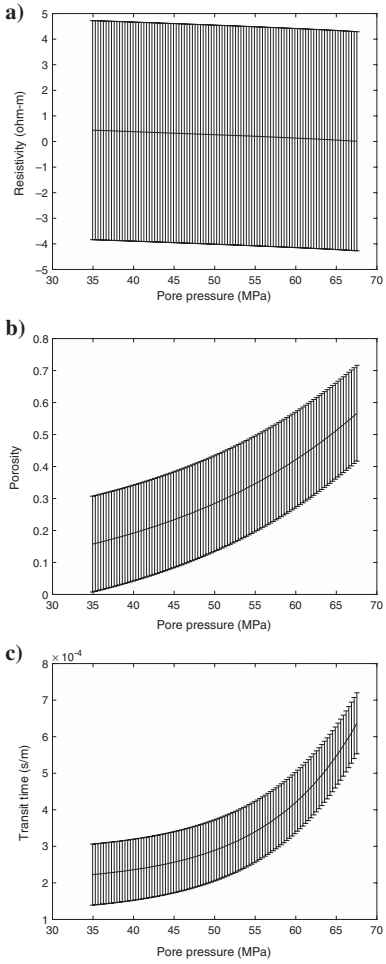

Figure 9. Likelihood equation 12 as a function of pore pressure at a fixed depth (3350 m) with vertical error bars (representing a 90% prediction interval). Here, the pore pressure varies between the hydrostatic pressure and the overburden stress at 3350 m. The figure helps in understanding the results obtained fitting the covariance matrix $\mathbf{R}$, showing the largest model error values for resistivity.

Using the transformed pore pressure variable as given in equation 2, we have the posterior distribution

$$\pi(\mathbf{x}|\mathbf{y}_1, \ldots, \mathbf{y}_j) = \frac{\pi(\mathbf{x})\pi(\mathbf{y}_1|\mathbf{x}) \ldots \pi(\mathbf{y}_j|\mathbf{x})}{\pi(\mathbf{y}_1, \ldots, \mathbf{y}_j)}$$
$$\propto \pi(\mathbf{x})\pi(\mathbf{y}_1|\mathbf{x}) \ldots \pi(\mathbf{y}_j|\boldsymbol{x}) \propto \pi(\mathbf{x}|\mathbf{y}_1, \ldots, \mathbf{y}_{j-1})\pi(\mathbf{y}_j|\mathbf{x}). \tag{21}$$

Here, we use the assumption that consecutive measurements along the borehole, for $j = 1, \ldots, N$, are conditionally independent, given the pore pressure variables; see equation 15. Meaning that the measurements, at a given location, depend only on the pore pressure at that location, and not on the variables at other locations. The distribution in equation 21 is assessed by a linearized approach, not dissimilar to the extended Kalman filter (Särkkä, 2013). This approach entails a linearization of the nonlinear expectation in the likelihood, with derivatives $\mathbf{G}_j = d\mathbf{g}_j/d\mathbf{x}$. The matrix $\mathbf{G}_j$ is an $m \times n$ matrix, where only the column corresponding to location $s_{w,j}$ is nonzero, whereas all other $n-1$ columns are zero. This structure is a result of the location-wise dependence.

For the situation with a Gaussian prior and a linearized Gaussian likelihood model, the sequential updating of data leads to a Gaussian distribution $\pi(\mathbf{x}|\mathbf{y}_1, \ldots, \mathbf{y}_j)$ in equation 21. The updated mean $\mathbf{m}_j = \mathbb{E}(\mathbf{x}|\mathbf{y}_1, \ldots, \mathbf{y}_j)$ and variance $\mathbf{V}_j = \mathrm{Var}(\mathbf{x}|\mathbf{y}_1, \ldots, \mathbf{y}_j)$ are computed recursively over the data gathering steps:

- Initialization:

$$\mathbf{m}_0 = \mu, \tag{22}$$

$$\mathbf{V}_0 = \Sigma. \tag{23}$$

- Recursive updating for $j = 1, \ldots, N$:

$$\begin{aligned} \mathbf{S}_j &= \mathbf{G}_j\mathbf{V}_{j-1}\mathbf{G}_j^t + \mathbf{R}, \\ \mathbf{K}_j &= \mathbf{V}_{j-1}\mathbf{G}_j^t\mathbf{S}_j^{-1}, \\ \mathbf{m}_j &= \mathbf{m}_{j-1} + \mathbf{K}_j(\mathbf{y}_j - \mathbf{g}_j(\mathbf{m}_{j-1})), \\ \mathbf{V}_j &= \mathbf{V}_{j-1} - \mathbf{K}_j\mathbf{G}_j\mathbf{V}_{j-1}. \end{aligned} \tag{24}$$

At the last step of the algorithm, we have the posterior Gaussian distribution $\pi(\mathbf{x}|\mathbf{y}_1, \ldots, \mathbf{y}_N)$, given all the data. Recall that several model assumptions have been done. First, we assume reliable predrill information for pore pressure that takes into account all the major mechanisms for pore pressure buildup and release. Moreover, the likelihood model is assumed to represent the well observations realistically.

RESULTS

We now present the results of the sequential updating method. The idea is to study a new case, in which we replay a well centered in a 3D subsurface grid (Figure 1) and study the effect of assimilating data. The regular grid is of size 10×10 in the northeast direction ((x, y) plane), where each compartment is 50×50 m^2.

In depth (the z-direction), we keep a structure similar to the one of the prior realization, with division in layers. Data are gathered along a vertical well, and the data assimilation starts at 1674 m and terminates at 3056 m.

Data $\mathbf{y}$ are simulated using first a realization from the prior and then a realization from the likelihood in equation 12. The sequential updating method, based on this data, is applied to $\mathbf{x}$ using equation 24. Results are visualized for pore pressure $\mathbf{p}$.

Figure 10 shows the results of the sequential updating procedure at an intermediate step, whereas Figures 11 and 12 compare the prior pore pressure distribution with the posterior distribution obtained at the final step. In Figure 10, we look at a step in which data are collected up to the depth of 2913 m. Figure 10a displays the pore pressure prediction for the sites along the well path with a 90% prediction interval. Hence, the true pore pressure would be covered by prediction interval approximately 90 out of 100 times. Figure 10b visualizes the updated SD and mean for a horizontal plane at depth 3056 m, which is 143 m ahead of the bit. The conditional mean and SD of pore pressure (in MPa units) are plotted for each grid site of the plane. We note how the smallest SDs are at the sites closer to the well location, due to the spatial dependence in the prior model.

Figure 11 shows a comparison between the prior and posterior SD in pore pressure in the 3D grid. The colorbars on the side of the plot are in MPa units. Again, the spatial dependence means that the reduction in the SD is larger in the area around the well (the white points), whereas it remains similar to the prior far from the well. Figure 12 shows a comparison between the prior (the black) and posterior (the magenta) pore pressure, along the well path. In this particular case, the well-log data indicate lower pore pressure than in the prior model, and the pore pressure predictive means are reduced. The reduction in the SD gives a narrower posterior prediction interval indicating that well-log data influence the pore pressure prediction.

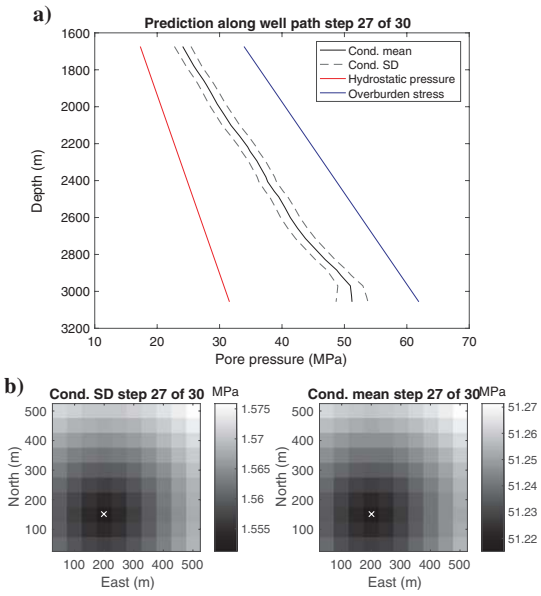

Figure 10. Intermediate step of the sequential updating; data are collected up to the depth of 2913 m. (a) Pore pressure along the well path with a 90% prediction interval. (b) SD (left) and mean (right) of pore pressure in each site of an horizontal plane at a depth of 3056 m, so 143 m ahead of the bit. The crosses indicate the well location. The lowest values of the SD are at sites closer to the well, due to the spatial dependency introduced in the prior covariance matrix.

DISCUSSION

A sensitivity analysis is carried out to study the impact of the prior and likelihood models on the results. We start by analyzing the effects of a variation of the fitted predrill assessment; we consider two variations of the prior covariance matrix. In the first situation (Case I), the covariance matrix keeps the same structure as in equation 7, but with $\sigma^2_{\text{new}} = 2 * \sigma^2$. This means that there will be greater prior uncertainty. For Case II, we include global variability in the prior. This is achieved by adding $\mathbf{z}\boldsymbol{\Sigma}_{\beta_{gl}}\mathbf{z}^T$ to the prior covariance $\boldsymbol{\Sigma}$. Here, $\mathbf{z}$ is a vector of all depth indices and $\boldsymbol{\Sigma}_{\beta_{gl}}$ represents the uncertainty (covariance matrix) for depth trends in pore pres-

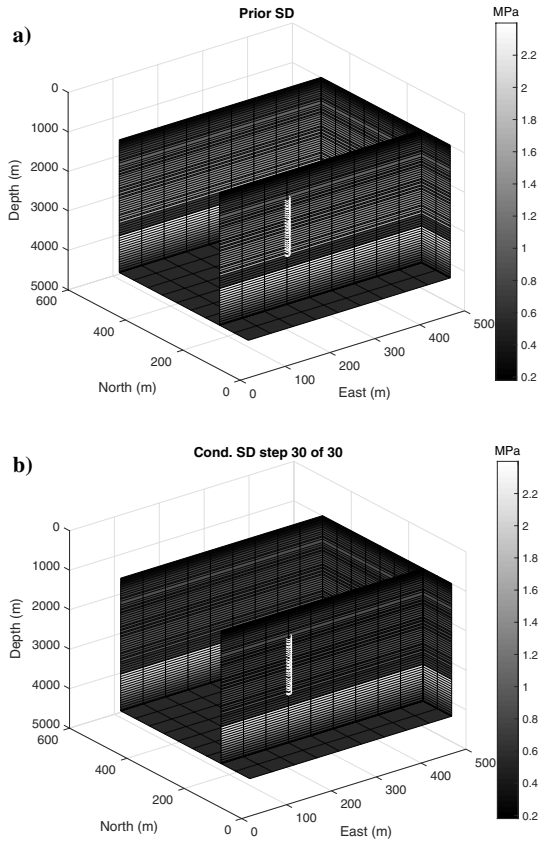

Figure 11. Comparison between (a) the prior and (b) the final pore pressure SD in a 3D grid of the area around the well (white points). There is a considerable reduction in the SD for the sites close to the well, whereas it remains similar to the prior for the sites that are farther.

sure, represented by a global regression line with intercept and slope. In this way, we include variabilities in the pore pressure depth trend. A third case (Case III) is considering the fact that faults are controlling the lateral fluid flow over geologic time, defining pressure compartments; i.e., fault patterns have a major control on the pressure distribution in a basin. Thus, the prior mean will depend not only on the depth but also on the pressure compartment. The replayed well situation is near the border of the two compartments in the top part of Figure 2b. In doing so, the pore pressure mean in the northern sites is obtained from one compartment, whereas southern sites have another compartment mean. The covariance matrix is obtained in the same way as for the base case.

To summarize, we have the following cases:

- Case I:
  $$\mathbf{\Sigma}_{\text{new}}(\mathbf{s}_{i,k},\mathbf{s}_{j,l}) = \sigma^2_{\text{new}} \exp\left(-\frac{\sqrt{(s_{i1,k}-s_{j1,l})^2+(s_{i2,k}-s_{j2,l})^2}}{r_1} - \frac{|s_{i3,k}-s_{j3,l}|}{r_2}\right),$$
  with $\sigma^2_{\text{new}} = 2 * \sigma^2$.
- Case II: $\mathbf{\Sigma}_{\text{new}} = \mathbf{\Sigma} + \mathbf{z}\mathbf{\Sigma}_{\beta_{gl}}\mathbf{z}^T$.
- Case III: Faults control the lateral fluid flow.

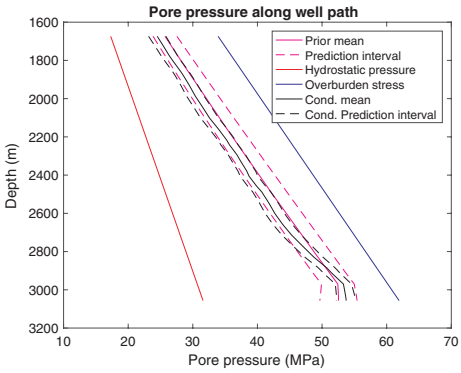

Figure 12. Prior and conditional pore pressure mean along the well path together with the respective prediction interval. There is a reduction in the uncertainty when the data assimilation procedure is complete; here, we can also spot a change in the pore pressure mean.

Table 2. Sensitivity to the prior model.

		SD values	
		143 m	0 m
Base case	Average SD	1.16	0.97
	SD at well site	1.47	0.93
Case I	Average SD	2.31	1.44
	SD at well site	2.28	1.37
Case II	Average SD	1.50	0.98
	SD at well site	1.48	0.95
Case III	Average SD	4.40	1.74
	SD at well site	4.39	1.65

The results are presented in Table 2, in which we report the SD at the planned well path site and the average SD in a horizontal plane at 143 and 0 m distance ahead of the bit.

With the larger prior uncertainty there is also a larger posterior SD, especially if we are far from the data acquisition point. When we get closer to the data acquisition point, the SD at the well site gets close to that of the base case. This can be seen as evidence of the ability of the method in reducing the uncertainty. If we look at the results of Case II in Table 2, we observe values very close to the base case. When we are 143 m from the plane, the SD is already relatively low because of the global effect term, in which updating ties up the model a bit faster.

To analyze Case III further, we plot the updated mean and SD in a horizontal plane, at the end of the well, in Figure 13. We see that the difference in pore pressure between the two compartments is very small in our case.

Because of the limited sealing capacity there is little effect here, but we suspect this could be more significant for other cases in which the lateral variation is larger.

We next study sensitivity to the likelihood model. First, we study the impact of the measurement error variance. The cases are

- Case IV: $\mathbf{R}_{\text{new}} = 4 * \mathbf{R}$.
- Case V: $\mathbf{R}_{\text{new}} = \frac{1}{4} * \mathbf{R}$.

Table 3 shows that less accurate measurements (Case IV) give a higher SD, relative to the base case. If we, vice versa, manage to get more accurate measurements, the SD is reduced, and this is particularly low in the area around the well where the data are collected.

To study which data types are more informative in our work, we analyze four different situations with subsets of data:

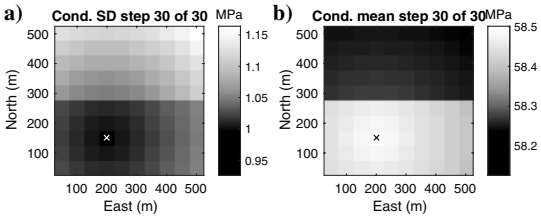

Figure 13. (a) The SD and (b) mean of pore pressure, the crosses indicate the well location. The pore pressure is showed in each site of an horizontal plane located at the same depth as the deepest point in the well. We capture the difference on pore pressure between the two compartments although the difference is small. This is due to the limited sealing capacity.

Table 3. Sensitivity to measurements error.

		SD values	
		143 m	0 m
Case IV	Average SD	1.52	1.24
	SD at well site	1.51	1.22
Case V	Average SD	1.31	0.69
	SD at well site	1.27	0.65

Table 4. Sensitivity to different data types.

		SD values	
		143 m	0 m
Case VI	Average SD	1.75	1.76
	SD at well site	1.75	1.76
Case VII	Average SD	1.70	1.45
	SD at well site	1.70	1.44
Case VIII	Average SD	1.75	1.75
	SD at well site	1.75	1.75
Case IX	Average SD	1.57	1.10
	SD at well site	1.56	1.05

- Case VI: only resistivity
- Case VII: only porosity (neutron porosity)
- Case VIII: only sonic transit time
- Case IX: porosity and sonic transit time

Table 4 shows the SD ratio values for different data types.

Studying the case with just resistivity (Case VI), the uncertainty in pore pressure is not reduced at all. In our case, the noise level is too large. Then, for cases with two data, we decide to exclude resistivity and only focus on porosity and sonic transit time. It is clear from Table 4 that having more data is better for accurate prediction of pore pressure because the SD decreases when more data are available. The transit time alone does not seem to be very informative (Case VIII), but when it is combined with porosity, the reduction of uncertainty is significant. Overall, as expected, porosity is the most informative data source for pore pressure, among the possible data studied here.

CONCLUSION

In this study, we build a prior model for pore pressure starting from predrill information of the field, and we use statistical techniques such as linear regression and variograms to incorporate trends and spatial dependencies in the model. Then, in the likelihood model, we fit links between the measurements and pore pressure. Finally, we sequentially update the pore pressure distribution with available measurements.

For the prior model, a predrill model for the pore pressure is used, resulting from pressure simulations over the geologic time scale (millions of years). The strength with this approach is that the effect of mechanical compaction and chemical compaction (illite-smectite transition in the shales) is simulated, in addition to the effect of lateral pressure transfer, mainly controlled by the fault properties and throw. Because sedimentary layers in the study are flat lying and the faults have minor throw, it results in little lateral variation in the simulated pressures. Larger lateral pressure differences are simulated and observed in other study areas such as the Halten Terrace, Norwegian Sea. We know that many of the input parameters hold large uncertainties; therefore, a Monte Carlo approach is preferred. In this study, only one simulation is used for the prior model.

The main contribution of this paper is pore pressure prediction highlighting the following points:

- Bayesian modeling: The approach provides consistent integration of predrill a priori knowledge about the pore pressure and the well-log measurements.
- Real time: The prediction of pore pressure is updated when the new well-log data are available.
- Spatial prediction: The prediction is not only done near the borehole location, but also ahead of the bit and at other lateral and depth locations.
- Uncertainty: The spatial predictions of pore pressure are represented by a mean value best prediction and a variance/covariance description.

The workflow we used for our particular case has a Gaussian prior model from predrill assessment. The linearized likelihood model for well logs allows efficient sequential Bayesian updating. Although this is a fit-for-purpose routine, the workflow is quite flexible and can be adapted in various situations. For instance, it can be applied to predrill assessment in which there are large uncertainties in depth trends, or for including other variables than pore pressure, such as more detailed information about facies classes. In addition, the measurements can include other kinds of data than what was considered here. One possibility is to evaluate the information content in formation tests, or look-ahead tools providing data for deeper locations. This can also be done in the context of improved decision making related to mud weight.

If Gaussian distributions are not realistic, another recursive updating method using stochastic simulations could be envisioned. The current workflow would then be extended to use realizations of pore pressure as the input and update these in real time when log data are available. We regard this as future work.

ACKNOWLEDGMENTS

The work is carried out as a part of the KPN project 255418/E30: "Reduced uncertainty in overpressures and drilling window prediction ahead of the bit (PressureAhead)" and is funded by the Norwegian Research Council and the DrillWell Centre (AkerBP, Wintershall, ConocoPhillips, and Statoil). ConocoPhillips contributed with input data.

DATA AND MATERIALS AVAILABILITY

Data associated with this research are confidential and cannot be released.

REFERENCES

Bektas, E., S. Z. Miska, E. M. Ozbayoglu, M. Yu, N. Takach, D. Velazquez-Cruz, and M. P. Shahri, 2015, Application of Kalman filter to predictions of pore pressure while drilling: Presented at the SPE Annual Technical Conference and Exhibition.

Bhakta, T., P. Avseth, and M. Landrø, 2016, Sensitivity analysis of effective fluid and rock bulk modulus due to changes in pore pressure, temperature and saturation: Journal of Applied Geophysics, **135**, 77–89, doi: 10.1016/j.jappgeo.2016.09.012.

Borge, H., 2000, Fault controlled pressure modelling in sedimentary basins: Ph.D. thesis, Norwegian University of Science and Technology.

Bowers, G. L., 1995, Pore pressure estimation from velocity data: Accounting for overpressure mechanisms besides undercompaction: SPE Drilling and Completion, **10**, 89–95, doi: 10.2118/27488-PA.

Chopra, S., and A. R. Huffman, 2006, Velocity determination for pore-pressure prediction: The Leading Edge, **25**, 1502–1515, doi: 10.1190/1.2405336.

Dobson, A. J., and A. Barnett, 2008, An introduction to generalized linear models: CRC Press.

Dutta, N., 2002, Geopressure prediction using seismic data: Current status and the road ahead: Geophysics, **67**, 2012–2041, doi: 10.1190/1.1527101.
Eaton, B. A., 1975, The equation for geopressure prediction from well logs: Presented at the Fall meeting of SPE of AIME, SPE.
Gholami, R., M. Rabiei, V. Rasouli, B. Aadnoy, and N. Fakhari, 2015, Application of quantitative risk assessment in wellbore stability analysis: Journal of Petroleum Science and Engineering, **135**, 185–200, doi: 10.1016/j.petrol.2015.09.013.
Goovaerts, P., 1997, Geostatistics for natural resources evaluation: Oxford University Press.
Jaeger, J., and N. Cook, 1963, Pinching-off and disking of rocks: Journal of Geophysical Research, **68**, 1759–1765, doi: 10.1029/JZ068i006p01759.
López, J. L., P. M. Rappold, G. A. Ugueto, J. B. Wieseneck, and C. K. Vu, 2004, Integrated shared earth model: 3D pore-pressure prediction and uncertainty analysis: The Leading Edge, **23**, 52–59, doi: 10.1190/1.1645455.
Lothe, A., 2004, Simulations of hydraulic fracturing and leakage in sedimentary basins: Ph.D. thesis, University of Bergen.
Lothe, A., H. Borge, and R. Gabrielsen, 2004, Modelling of hydraulic leakage by pressure and stress simulations and implications for Biot's constant: An example from the Halten terrace, offshore Mid-Norway: Petroleum Geoscience, **10**, 199–213, doi: 10.1144/1354-079303-579.
Lothe, A., P. Cerasi, K. Bjørkevoll, and S. Haavardstein, 2018, Digitized uncertainty handling of pore pressure and mud-weight window ahead of bit; example North Sea: IADC/SPE Drilling Conference and Exhibition, IADC/SPE-189665–MS.
Lothe, A., and A. Grøver, 2009, Evaluation of sealing properties to faults and cap rocks and its influence on fluid pressure distribution — Using a Monte Carlo simulation approach: Presented at theAAPG Hedberg Research Conference.
Malinverno, A., and R. L. Parker, 2006, Two ways to quantify uncertainty in geophysical inverse problems: Geophysics, **71**, no. 3, W15–W27, doi: 10.1190/1.2194516.
Malinverno, A., C. M. Sayers, M. J. Woodward, and R. C. Bartman, 2004, Integrating diverse measurements to predict pore pressure with uncertainties while drilling: Presented at theSPE Annual Technical Conference and Exhibition.
Mavko, G., T. Mukerji, and J. Dvorkin, 2009, The rock physics handbook: Tools for seismic analysis of porous media: Cambridge University Press.
Oughton, R. H., D. A. Wooff, R. W. Hobbs, R. E. Swarbrick, and S. A. O'Connor, 2017, A sequential dynamic Bayesian network for pore pressure estimation with uncertainty quantification: Geophysics, **83**, no. 2, D27–D39, doi: 10.1190/geo2016-0566.1.
Rommetveit, R., K. S. Bjorkevoll, P. R. Cerasi, S. T. Havardstein, M. Fjeldheim, H. M. Helset, S. I. Odegard, and C. Nordstrand, 2010, Real time integration of ECD, temperature, well stability and geo/pore pressure simulations during drilling a challenging HPHT well: Presented at theSPE Intelligent Energy Conference and Exhibition.
Särkkä, S., 2013, Bayesian filtering and smoothing: Cambridge University Press.
Sayers, C., L. Den Boer, Z. Nagy, P. Hooyman, and V. Ward, 2005, Pore pressure in the Gulf of Mexico: Seeing ahead of the bit: World Oil, **55**, 55–58.
Sayers, C. M., G. Johnson, and G. Denyer, 2002, Predrill pore-pressure prediction using seismic data: Geophysics, **67**, 1286–1292, doi: 10.1190/1.1500391.
Sclater, J. G., and P. A. Christie, 1980, Continental stretching: An explanation of the post-mid-cretaceous subsidence of the central North Sea basin: Journal of Geophysical Research: Solid Earth, **85**, 3711–3739, doi: 10.1029/JB085iB07p03711.
Twiss, R. J., and E. M. Moores, 1992, Structural geology: Macmillan.
Ugwu, G., 2015, An overview of pore pressure prediction using seismically derived velocities: Journal of Geology and Mining Research, **7**, 74–80, doi: 10.5897/JGMR15.0218.
Walderhaug, O., 1996, Kinetic modeling of Quartz cementation and porosity loss in deeply buried sandstone reservoirs: AAPG Bulletin, **80**, 731–745.
Wessling, S., A. Bartetzko, and P. Tesch, 2013, Quantification of uncertainty in a multistage/multiparameter modeling workflow: Pore pressure from geophysical well logs: Geophysics, **78**, no. 3, WB101–WB112, doi: 10.1190/geo2012-0402.1.
Zhang, J., 2011, Pore pressure prediction from well logs: Methods, modifications, and new approaches: Earth-Science Reviews, **108**, 50–63, doi: 10.1016/j.earscirev.2011.06.001.

Uncertainties in mud-weight window for safe drilling operations

Jacopo Paglia, Jo Eidsvik, Pierre Cerasi

Under revision in SPE Journal

This paper is awaiting publication and is not included in NTNU Open

Efficient spatial designs using Hausdorff distance and Bayesian optimization

Jacopo Paglia, Jo Eidsvik, Juha Karvanen

Submitted to Scandinavian Journal of Statistics

This paper is awaiting publication and is not included in NTNU Open

ISBN 978-82-326-4692-0 (printed version)
ISBN 978-82-326-4693-7 (electronic version)
ISSN 1503-8181

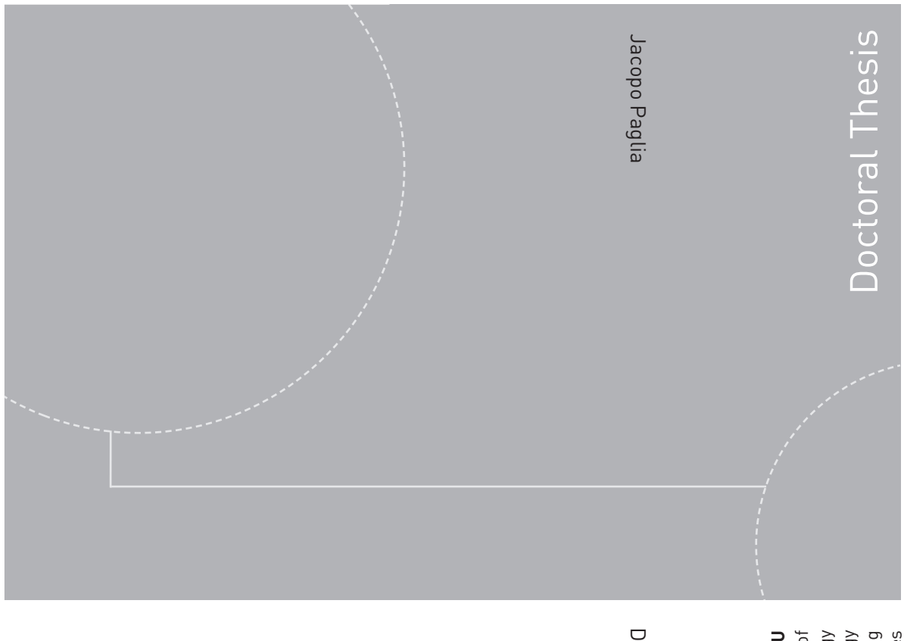

Doctoral theses at NTNU, 2020:172

Jacopo Paglia

Statistical modeling for safer drilling operations

NTNU
Norwegian University of
Science and Technology
Faculty of Information Technology
and Electrical Engineering
Department of Mathematical Sciences

NTNU
Norwegian University of
Science and Technology

Doctoral theses at NTNU, 2020:172

NTNU

NTNU
Norwegian University of
Science and Technology